

^{97}Tc produced by the ($^3\text{He},pn\gamma$) reaction

Hurol Aslan,* Ben Crowe,† Tim Dague, D. G. Savage,‡ Sadek Zeghib,§ F. A. Rickey, and P. C. Simms
Tandem Accelerator Laboratory, Department of Physics, Purdue University, Lafayette, Indiana 47907

(Received 8 November 1995)

The nuclear structure of ^{97}Tc was studied using the $^{96}\text{Mo}(^3\text{He},pn\gamma)$ reaction, which has populated most states in the nucleus below 2 MeV excitation energy. The proton exit channel was isolated from competing reaction channels by operating γ -ray detectors in coincidence with a large-solid-angle proton detector. The experiments included γ -ray excitation functions, γ -ray angular distributions, and γ - γ coincidences. The results were interpreted using a particle-rotor model. [S0556-2813(96)04208-2]

PACS number(s): 23.20.Lv, 23.20.En, 25.55.Hp, 27.60.+j

I. INTRODUCTION

The use of the spherical shell model to interpret the structure of closed-shell nuclei is generally accepted. Far from closed shells (particularly in the rare earth and actinide regions) nuclei exhibit regular rotational bands accepted as evidence for large permanent deformations. Between these extremes lie the so-called transitional nuclei. It seems probable that deformations must exist in transitional nuclei, but the questions of where they exist, and their magnitudes, are intriguing. The traditional view has been that vibrations about spherical shapes are the dominant collective degree of freedom near closed shells, and that collective rotations do not set in until the nuclei are further from closed shells. But the recognition of rotational features can be obscured because the Coriolis interaction, which is an integral part of rotational models, can distort the familiar patterns of rotational bands. In fact vibrational models and rotational models can provide similar interpretations of states near the yrast line in transitional nuclei. Hence heavy-ion reactions, which preferentially populate yrast states, do not distinguish between these models. On the other hand, we have found [1,2] that most states in a nucleus below 2 MeV excitation can be observed using ^3He fusion reactions with projectile energy a few MeV above the Coulomb barrier. Technetium nuclei are interesting because they span a transition region. ^{93}Tc (with 50 neutrons) appears to be spherical while ^{101}Tc (with 58 neutrons) has many properties expected for a deformed nucleus. This paper reports our investigation of ^{97}Tc . Since we have approximately doubled the known states below 2 MeV, this experiment provides a more complete data set which can be used to evaluate the competing models of transitional nuclei.

A previous study of ^{97}Tc [3] utilized the interacting boson

fermion model (IBFM) [4] to interpret positive-parity states near the yrast line. This calculation was performed in the near-vibrational limit. An alternate approach is to consider collective rotations. Previous work [1,2,5] has suggested that collective rotations are the dominant collective degree of freedom in neighboring nuclei. Accordingly, we have used a symmetric-rotor model for our interpretation of the data. This approach has the advantage of simplicity. The transition in Tc nuclei from deformed to spherical can be treated simply as a change in deformation. The model utilizes a rotational Hamiltonian in the strong coupling limit modified to include a variable moment of inertia [6]. Pairing is treated by the BCS formalism. The Coriolis and recoil terms are treated to all order. This basic model has been used for years to interpret strongly deformed nuclei.

The $^{96}\text{Mo}(^3\text{He},pn\gamma)^{97}\text{Tc}$ reaction was used in this experiment. A large-solid-angle proton detector was operated in coincidence with γ -ray detectors to separate the pn exit channel from xn and αxn channels. The improvement in the data was striking, which permitted us to see many weak γ -ray transitions that would have been lost without the proton gate. An electronic system was developed to handle γ -ray counting rates in excess of 100 000 per sec, so that adequate statistical errors could be obtained for low intensity γ rays in a reasonable time.

The measurements include γ -ray excitation functions, angular distributions, and γ - γ coincidences. The degree of nuclear orientation observed in these experiments is lower than that obtained with heavy-ion reactions, hence spin assignments based on angular distributions can be less definite. However, the γ -ray excitation function can be used with the angular distribution to make spin assignments, as will be discussed later. Measurements for many weak γ rays were distorted by other γ rays with similar energy. This problem was minimized by using directional correlations in the coincidence data to make spin assignments.

II. EXPERIMENTAL TECHNIQUES

The target was a foil of isotopically enriched ^{96}Mo rolled to a uniform thickness of 1.3 mg/cm². The composition was 96.8% ^{96}Mo with 1% impurities of $^{95,97,98}\text{Mo}$. The ^3He beam currents of 10–25 nA were supplied by the Purdue FN Tandem Van de Graaff accelerator.

The two hyperpure Ge γ -ray detectors used had energy

*Present address: Department of Nuclear Engineering, Hacettepe University, Ankara, Turkey.

†Present address: Triangle Universities Nuclear Laboratory, Durham, NC 27706.

‡Present address: Department of Physics, Hampton University, Hampton, VA 23668.

§Present address: Institut des Sciences Exactes et Technologie, Université de Constantine, Constantine, Algeria.

resolutions of ~ 2.0 keV at 1332 keV and efficiencies of $\sim 20\%$. The energy signals from the detectors were processed by ORTEC 673 spectroscopy amplifiers and ORTEC AD413 analog-to-digital converters. A ^{152}Eu radioactive source was used for energy calibration and to measure the change in detector efficiency as a function of energy. Eight γ rays were used to construct a linear calibration. The rms deviation of the known energies [7] from the calibration was 44 eV.

The energy calibration was monitored in beam using γ rays with known energy from the ^{197}Au beam stop and a ^{60}Co radioactive source placed near the detectors. The observed energies for these γ rays varied less than 100 eV during each measurement.

Data were collected on a DEC Micro Vax 3400 computer through a CAMAC interface. The interface used a Kinetics Systems Model 3982 List Sequencing Crate Controller to collect data in a 4096 word memory for batch transfer to the computer, minimizing dead time. The system can accept approximately 50 000 proton- γ coincidence events per sec or 30 000 proton- γ - γ coincidence events per sec.

Two proton detectors were used, one above and one below the target. Each detector had a solid angle of approximately 33%. The detectors were 0.001-in.-thick plastic scintillators mounted on RCA 8575 photomultiplier tubes. These thin scintillators provided ample signals for proton detection, but they had very low detection efficiency for γ rays. The scintillators were covered with thin lead foil to prevent detection of α particles and ^3He .

Two techniques were used to facilitate high γ -ray counting rates. The ^3He beam was electrostatically deflected off the target as soon as a γ ray was detected to minimize the probability of pulse pileup from subsequent γ rays. The beam was held off the target until the accepted event was processed. Accurate dead time corrections are difficult with the pulsed beam, so a lower intensity, continuous beam was used for the angular distribution measurement. The ORTEC 673 spectroscopy amplifier includes a gated integrator, in addition to the usual active filter, to improve the signal-to-noise ratio. The addition of the gated integrator reduced the amplifier pulse width by 60% with negligible loss in γ -ray energy resolution. These techniques permit efficient data collection with average γ -ray counting rates of approximately 100 000 per sec.

Time-to-amplitude converters (TAC's) were used in the coincidence system. The TAC was started by the γ -ray detector and stopped by the proton detector. Two TAC's were required for the proton- γ - γ coincidence system. A separate digital logic circuit ensured that the same proton pulse stopped both TAC's. The TAC spectra were processed in the on-line computer so that flexible windows could be used to define true and accidental coincidences. The time jitter of the pulse from the γ -ray detector system is inversely proportional to the energy of the γ ray. Therefore, the window widths were adjusted as a function of the γ -ray energy for each coincidence event to optimize the true-to-chance ratio. The true and chance windows always had the same width. Accidental coincidences were subtracted as the data were accumulated. The window width varied from about 70 nsec for 50 keV γ rays to 10 nsec for γ rays with energy above 500 keV.

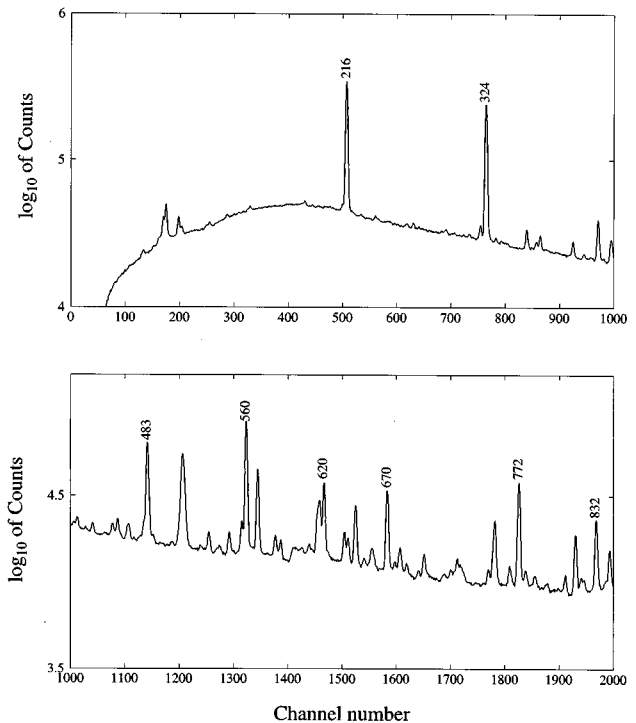


FIG. 1. A portion of a proton-gated singles spectrum from the $^{96}\text{Mo}(^3\text{He},pn\gamma)^{97}\text{Tc}$ reaction at a laboratory energy of 18 MeV.

The time jitter for low energy γ rays is so large that many of them are lost in a coincidence experiment. Elron STD-N-1 snapoff triggers were used for the γ -ray timing signals. The coincidence efficiency was approximately 35% for an 80 keV γ ray. The efficiency increases to 100% for γ -ray energies above 200 keV.

The chance coincidence spectrum from a start-stop TAC has an exponential shape because more than one stop pulse can occur within the range of the TAC. This effect would cause a 9% error in chance coincidence subtraction at the high counting rates used in these experiments. The effect was removed by introducing a fixed dead time in the stop input of the TAC.

A. Excitation functions

Proton-gated singles spectra were recorded at 13.5, 15, 16.5, and 18 MeV. A typical spectrum is shown in Fig. 1. These measurements served the dual functions of selecting the appropriate beam energy for subsequent experiments and providing spin information, as discussed in the next section. The angular distribution and γ - γ coincidence experiments were run at 18 MeV. The primary reason for this choice was to optimize the ($^3\text{He},pn$) reaction relative to other reactions that follow the breakup of ^3He in the Coulomb field of the nucleus. This process also produces ^{97}Tc but provides lower nuclear orientation. The ^{96}Ru γ rays from the $3n$ exit channel substantially increased the total γ -ray counting rate, but they were excluded from the proton-gated spectrum used to study ^{97}Tc . ^{97}Mo γ rays from the $2p$ exit channel were included in the proton-gated spectrum, but they were much weaker than the ^{97}Tc γ rays.

B. Angular distributions

The angular distribution measurement consisted of proton-gated singles spectra collected at 0° , 45° , and 90° with respect to the beam line. The angular distribution coefficients, A_{kk} , were extracted using a least squares procedure and corrected for the detector solid angle. Particle and γ -ray emission reduces the original alignment of the compound system so that the experimental coefficients A_{kk} are smaller than the theoretical ones A_{kk}^0 .

$$A_{kk} = \alpha_k A_{kk}^0 \quad (1)$$

Typical values of α_k must be obtained from the experimental data using unmixed $E1$ and $E2$ transitions between states of known spin. Low-spin states are less orientated than high-spin states. α_2 varied in this experiment from approximately 0.2 for spin $5/2$ to approximately 0.8 for spin $17/2$. The α_4 is much smaller than α_2 , hence the A_{44} coefficient usually was negligible for the orientations obtained in these experiments.

C. γ - γ coincidence measurement

The coincidence measurement was performed using two detectors positioned at 0° and 100° with respect to the beam axis. The data were stored as a 4096×4096 array in the computer memory. One-dimensional projections of the array were also accumulated (i.e., all γ rays in one detector that are coincidence with any γ ray in the other detector). A somewhat novel approach was used to process the coincidence data. It is a modification of a direct decomposition scheme reported earlier [8], which works with the complete γ - γ coincidence matrix, rather than parts of the coincidence matrix condensed into one-dimensional gate spectra. We believe that direct decomposition has advantages over the gate spectra method, both in flexibility and accuracy.

Our version of the direct decomposition method starts with least squares fits to all peaks in the two projections. The centroids and widths of all photopeaks are determined in this process, and held fixed in subsequent stages of the analysis. The total coincidence matrix is divided into submatrices, with the criteria that there are no overlaps between peaks in the different submatrices. A three-dimensional linear least squares fit is then performed to the data in each submatrix, to simultaneously determine (1) the background, (2) the Compton ridges in both directions, and (3) the peak areas. This fit runs reliably and automatically, and can readily be repeated for isolated sections of the complete array, after adding, deleting, or modifying peaks. If gate spectra are desired for any special purpose, like checking centroids, they can be constructed with ease.

We rely on the coincidence results not only for yes-no criteria as to which γ transitions are in coincidence, but also for angular-momentum determinations and γ -ray intensities. Peak areas extracted in the fitting process were corrected for (1) γ -ray detector efficiency as a function of γ -ray energy, (2) γ -ray absorption in the chamber walls and detector windows, and (3) losses at low γ -ray energy due to the timing circuits used with the γ -ray detectors.

III. THE LEVEL SCHEME

The level scheme deduced in the present work for ^{97}Tc is shown in Figs. 2, 3, 4, and 5. The low background in the proton-gated coincidence data allowed the placement of many weak transitions. 191 γ rays were identified as belonging to ^{97}Tc and placed unambiguously in the level scheme. The level scheme contains 110 states, 45 of which are new.

A tabular form of the level scheme is given in Table I. New states are marked with a superscript “*a*” following their energy. Most γ rays were placed by coincidence with γ rays that precede and follow in the decay pattern. In some cases several γ rays were assigned to the same state on the basis of energy agreement, because the observed feeding to the state was too weak to provide coincidence confirmation (indicated by superscript “*b*” on the γ -ray energy). A superscript “*c*” on the γ -ray energy means that the γ ray was placed between known states by energy agreement only. The observed feeding to the initial state was too weak to provide coincidence confirmation, and the final state was the ground state or the 96.60-keV isomeric state.

The precision of most γ -ray energy measurements was approximately 50 eV. Less accurate measurements are indicated by significant figures. The 949.9-keV and 1366.2-keV γ rays from the states at 1274.48 keV and 1581.95 keV, respectively, were placed tentatively by an energy match, although the energy uncertainty was 1.8 keV and 1.2 keV, respectively.

The spin and parity assignments are based on a combination of several sources: previous works [3,9], previous data compiled in Nuclear Data Sheets (NDS) [10], γ -ray branching patterns, and our analysis of excitation functions, angular distributions, and directional correlations in the coincidence data. Many new spin assignments were made and others were confirmed that had been considered tentative in NDS [10]. Ambiguity in spin assignment is indicated by multiple spin values. A tentative assignment is shown in parenthesis.

A γ -ray excitation function depends on the angular momentum of the state from which it is emitted. The excitation functions were normalized to that of the 861.75-keV transition to the ground state in ^{97}Tc to remove the common energy dependence. Then the γ -ray intensity was fitted to an exponential function of energy:

$$I_\gamma \propto e^{bE}. \quad (2)$$

The exponential “slope” b is approximately proportional to the angular momentum of the state. (Variations of this technique are common [11,12].)

Equal slope intervals were used to estimate the angular momentum, as listed in Table II. A different set of intervals was necessary for positive- and negative-parity states. The spin of 20 states can be determined without using the excitation-function data. The excitation-function slope for 18 of these 20 states fall within the intervals given in Table II. There are two exceptions. The spin of the 994.58-keV state is $3/2^+$, but the slope suggests $5/2^+$. The spin of the 1849.56-keV states is $15/2^+$, but the slope suggests $13/2^+$. The “data used” column in Table I has an E when the excitation function was used to help assign angular momentum and parity to a state.

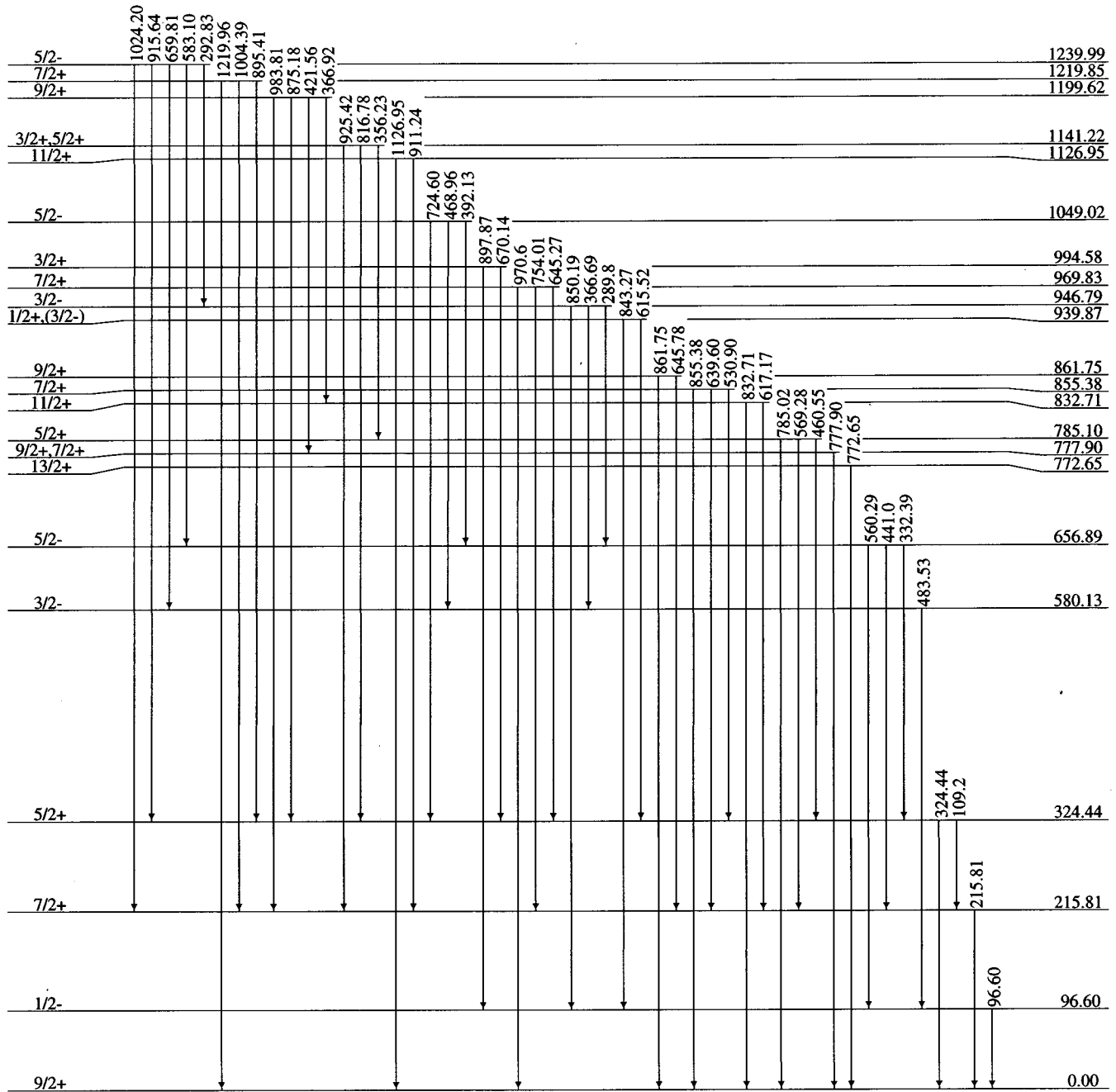


FIG. 2. The low energy portion of the level scheme deduced for ^{97}Tc . Note that the vertical energy scale is not linear.

The angular distribution data were used to restrict angular momentum and parity choices. Only the general size and sign of the A_{22} was used because the degree of nuclear orientation was not well known. The measured A_{22} values are listed in Table I.

Additional angular momentum information was obtained from DCO analysis [13,14] of the coincidence data. (DCO stands for γ - γ directional correlation from oriented nuclei.) The DCO has the advantage that it is much less likely to be affected by unresolved γ rays. Complete DCO analysis [13] was performed to make spin assignments, but the DCO ratio was not given in Table I. Instead, we have calculated the value of A_{22} that the γ ray would have for the spin sequence

and mixing ratio required by the experimental DCO ratio. Then the angular distribution and DCO measurements can be evaluated on the same basis. These "implied" A_{22} values are listed in Table I. The "data-used" column of Table I tells when the angular distribution (A) or DCO (D) was used in the spin analysis. A " π " subscript is added to A or D when the measurement excludes parity change for the γ transition.

Most spin and parity assignments are based on γ rays that depopulate the state, but γ rays that feed a state are also useful. For example, consider the 969.83-keV state. The 215.81-keV and 324.44-keV γ rays that depopulate the state restrict the spin to $5/2^+$ or $7/2^+$. This ambiguity is removed by the 752.4-keV transition from the $5/2^+$ state at 1721.9

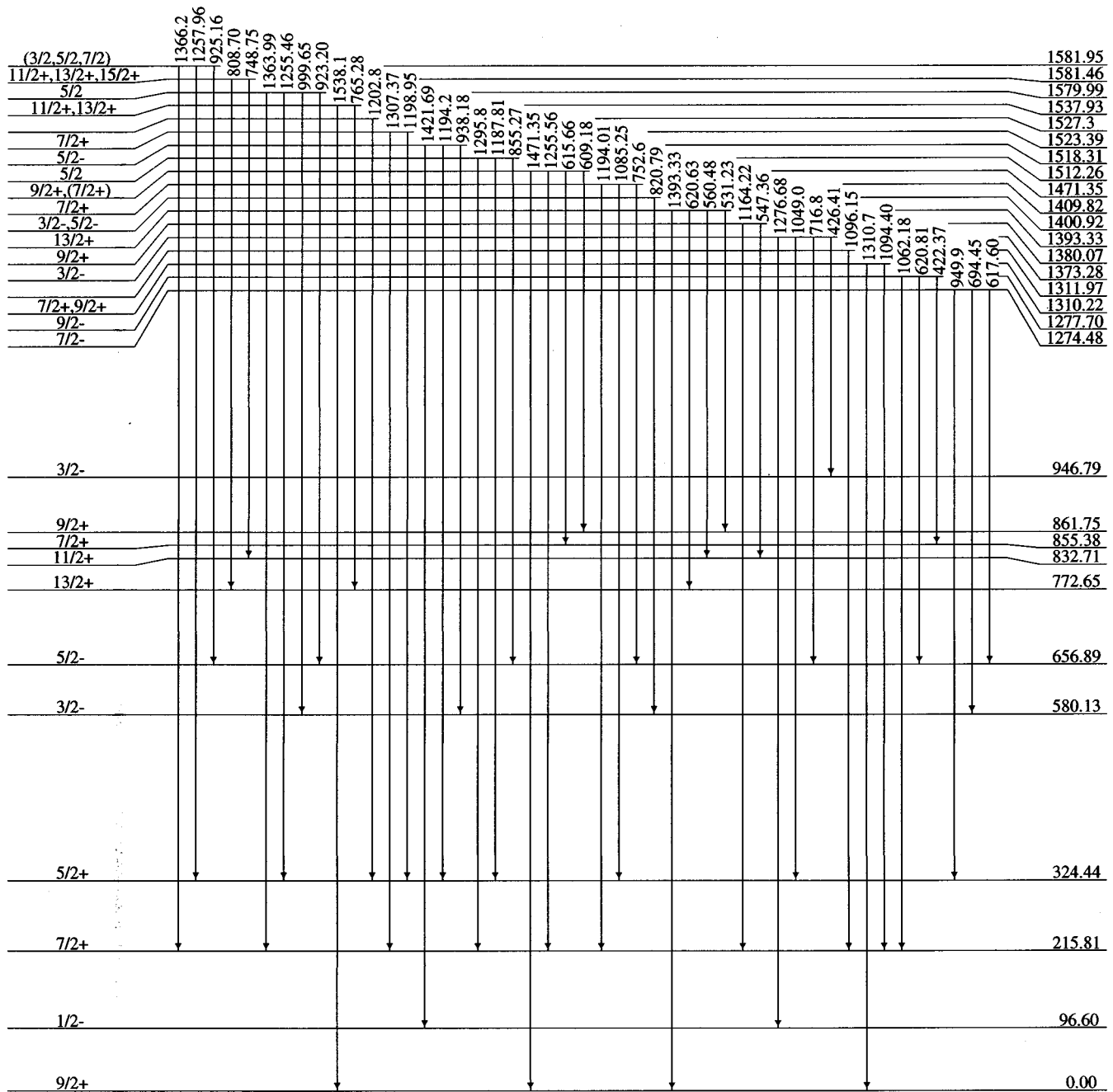


FIG. 3. A middle energy portion of the level scheme deduced for ^{97}Tc . The energy scale is not linear.

keV to the 969.83-keV state. The DCOQ of the 752.4-keV γ -ray shows that it changes spin by one unit, hence the 969.83-keV state must be $7/2^+$ not $5/2^+$. The $5/2^+$ spin assignment for the 1721.9-keV state is independent of the $5/2^+$ or $7/2^+$ choice for the 969.83-keV state.

The γ -ray intensity was taken from the angular distribution measurement, unless the coincidence analysis showed that there was a second γ ray unresolved from the γ ray of interest. In that case, the intensity was taken from the coincidence analysis.

Our results for several levels are inconsistent with previous publications. The 617.17-keV and 832.71-keV γ rays that depopulate the 832.71-keV level are assigned to different levels in Ref. [3]. However, both γ rays are in coinci-

dence with the γ rays that populate the 832.71-keV level, hence both must be coming from the 832.71-keV level. In our level scheme the 441.0-keV γ ray depopulates the 656.89-keV level rather than a 765.71-keV level reported in Ref. [3]. In our data this γ ray is in coincidence with the 215.81-keV γ ray but not the 324.44-keV γ ray.

NDS [10] assigned spin $3/2^-$ to the 1049.02-keV level. Our angular distribution and DCOQ measurements for the 724.60 γ ray gives a positive A_{22} , which is inconsistent with a $3/2^-$ to $5/2^+$ transition. Our measurements require a spin assignment of $5/2^-$, as shown in Table I.

The level we observed at 1373.28 keV apparently is not the same as the level reported in NDS [10] at 1372.3 keV. Three γ rays we observed coming from this state had slightly

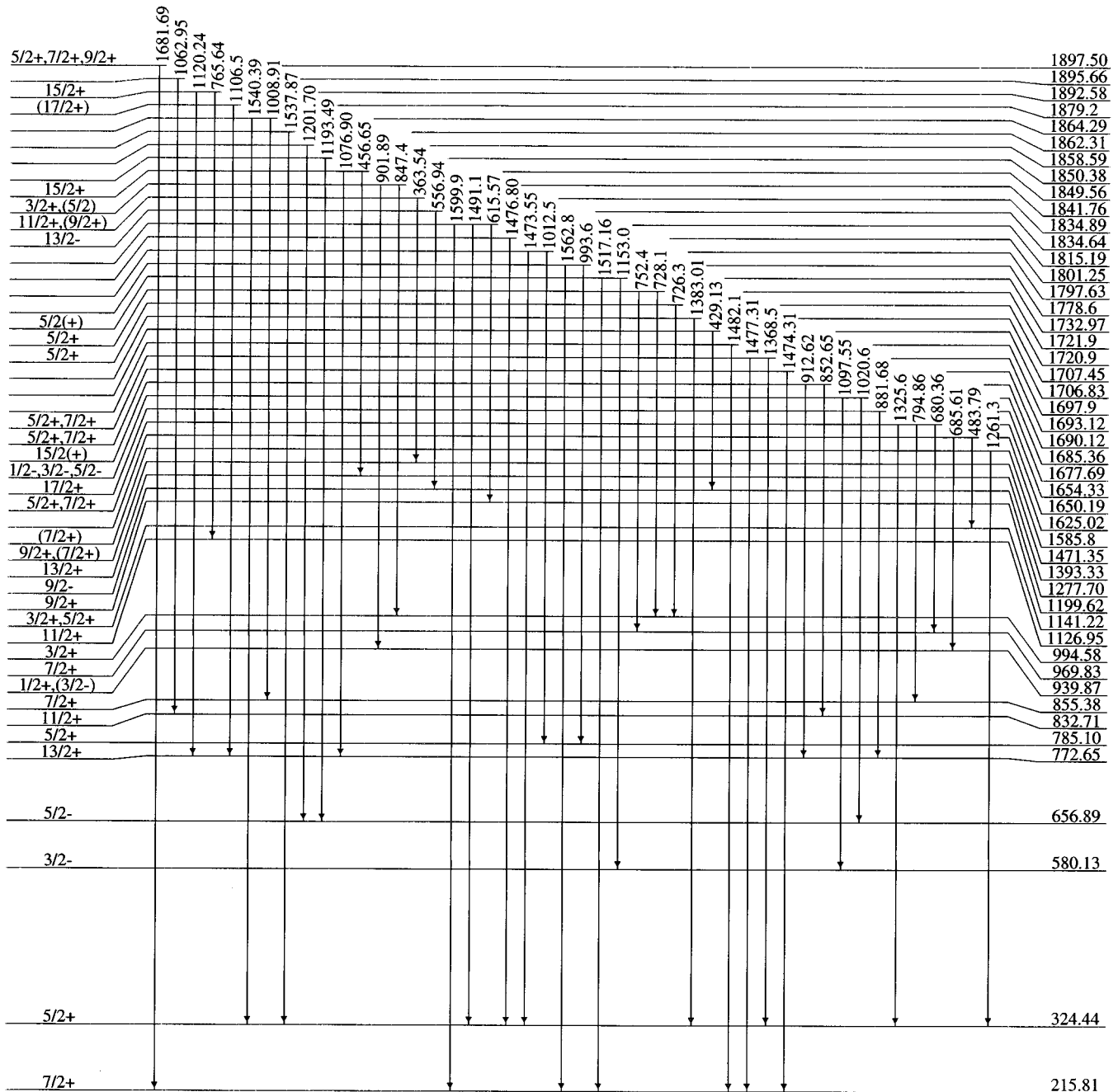


FIG. 4. A middle energy portion of the level scheme deduced for ^{97}Tc .

higher energies (716.8, 1040.9, and 1276.68 keV) than three similar γ rays reported in NDS [10] (715.9, 1048.0, and 1275.0 keV). In most cases our γ -ray energies agree with the NDS values to within 200 eV or less. Furthermore, the relative intensities for the three γ rays are not the same here as in NDS [10]. Finally, we observe a 426.41-keV γ ray emitted from the state that NDS did not report, and NDS reported a 1054-keV γ ray that we did not observe.

IV. DISCUSSION AND INTERPRETATION

The level scheme of ^{97}Tc is marked by the $9/2^+$ ground state and low-lying $7/2^+$, $5/2^+$, $1/2^-$, $3/2^-$, and $5/2^-$ states.

The IBFM calculation cited earlier [3] accounted for the positive-parity states of this group, as well as selected higher-lying positive-parity states near the yrast line. The association of model states with experimental states is difficult to evaluate, since no transition probabilities were calculated, and only energy matches can be considered. Some of the matches are within 100 keV, while other energy differences (approximately half of them) are between 100 and 350 keV. This energy agreement for models of this sort is reasonable, but not definitive. No interpretation of negative-parity states was presented. In an alternative approach, the occurrences of these states at low excitation energies follow naturally if ^{97}Tc is deformed. The Nilsson [15] diagram ap-

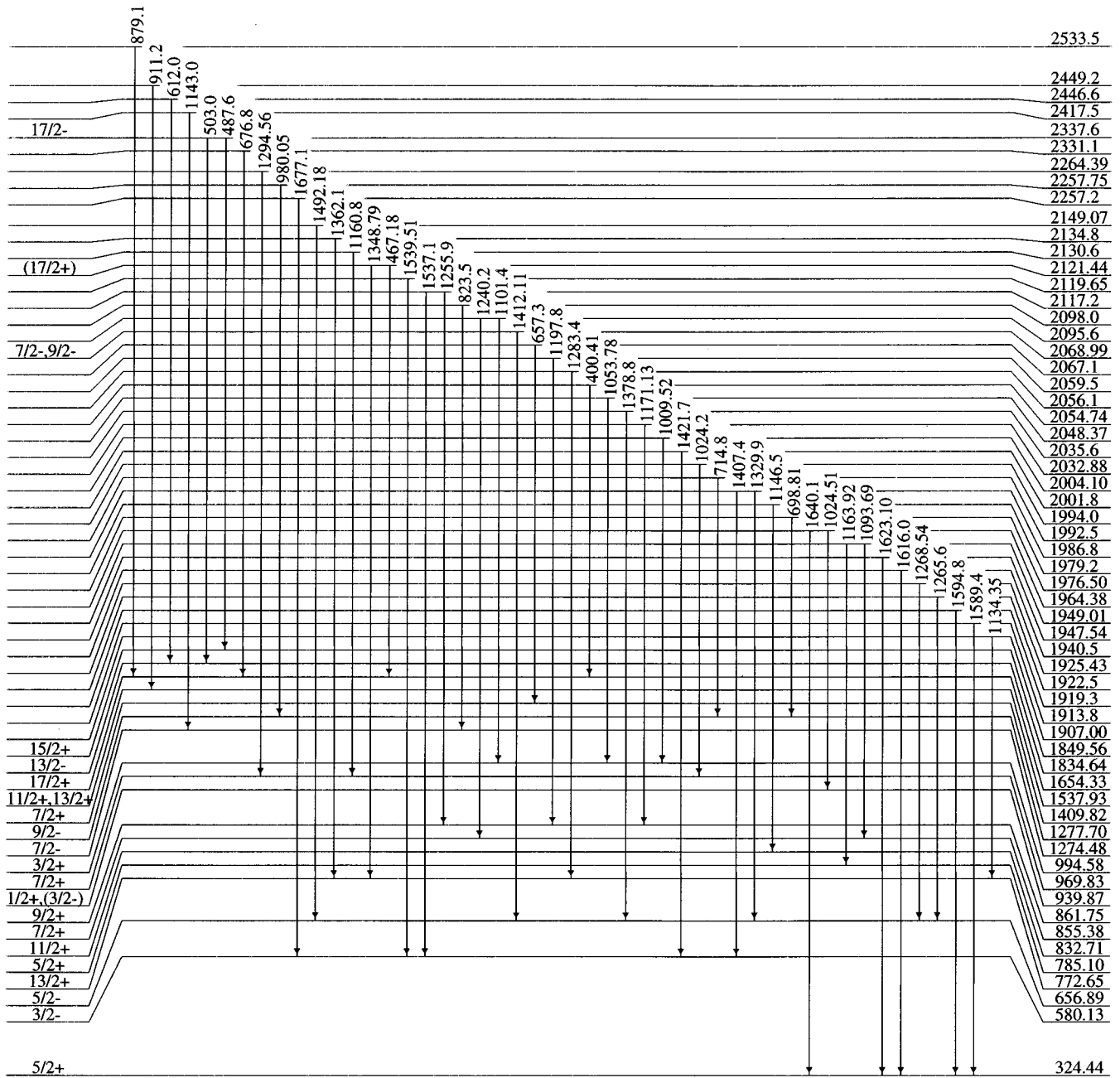


FIG. 5. The higher energy portion of the level scheme deduced for ^{97}Tc .

appropriate for odd protons in ^{97}Tc is shown in Fig. 6. Since ^{97}Tc has 43 protons, the Fermi surface would lie near Nilsson states of spins $5/2+$, $1/2-$, $3/2-$, and $5/2-$ for deformations greater than $\delta = 0.15$. In the simplest Nilsson picture, the $7/2+$ and $9/2+$ members of a $5/2+[422]$ rotational band would also lie at low excitation energies. When the Coriolis interaction is included, states of these spins can be depressed in energy below the lowest $5/2+$ state. In addition the $1/2+$ and $3/2+$ states at 939.87 keV and 994.58 keV, respectively, are indications of a still higher deformation. At deformations greater than $\delta = 0.18$, the $Z = 50$ shell closure disappears, and the $1/2+[431]$ Nilsson state approaches the Fermi surface. (A similar situation was found in ^{111}Ag [2].) For these reasons the use of a rotational model for the interpretation of

the structure observed in ^{97}Tc seemed natural. A great strength of this model is that electromagnetic transition properties can be readily calculated. These can be used in the comparison of calculated and experimental results. Energies alone are not a sufficient basis for comparison, since small perturbations to any model can have relatively large effects on the calculated energies, and frequently there are several experimental states of the same spin and parity which have similar excitation energies. The same perturbations generally affect wave functions less, thus the comparison of experimental and calculated branching ratios strengthens the identification.

The rotational model used was a symmetric particle-plus rotor model. The calculation of energies and wave functions

TABLE I. Analysis of γ rays emitted following the $^{96}\text{Mo}(^3\text{He},pn)^{97}\text{Tc}$ reaction at 18 MeV.

| E_i (keV) | I_i^π | E_γ (keV) | I_f^π | E_f (keV) | Intensities | | A_{22} $\times 100$ | Exc. func. | Data used ^d |
|---------------------|----------------------------------|----------------------|------------------|----------------|------------------|-------|--------------------------|---------------|---------------------------|
| | | | | | ^{97}Tc | Other | | | |
| 96.60 | $\frac{1}{2}^-$ | 96.60 | $\frac{9}{2}^+$ | 0.00 | | | | | <i>N</i> |
| 215.81 | $\frac{7}{2}^+$ | 215.81 | $\frac{9}{2}^+$ | 0.00 | 2002 | | -11(2) | -110(2) | <i>E,A</i> |
| 324.44 | $\frac{5}{2}^+$ | 324.44 | $\frac{9}{2}^+$ | 0.00 | 1910 | | 4(2) | -146(2) | <i>E,A,A_\pi</i> |
| | | 109.2 | $\frac{7}{2}^+$ | 215.81 | 17 | | -7(16) | -148(30) | |
| 580.13 | $\frac{3}{2}^-$ | 483.53 | $\frac{1}{2}^-$ | 96.60 | 664 | 53 | -6(2) | -125(3) | <i>E,A</i> |
| 656.89 | $\frac{3}{2}^-$ | 560.29 | $\frac{1}{2}^-$ | 96.60 | 968 | 32 | 13(2) | -49(2) | <i>E,A,A_\pi</i> |
| | | 332.39 | $\frac{5}{2}^+$ | 324.44 | 11 | | 44(18) | | |
| | | 441.0 | $\frac{7}{2}^+$ | 215.81 | 6 | 20 | | | |
| 772.65 | $\frac{13}{2}^+$ | 772.65 | $\frac{9}{2}^+$ | 0.00 | 557 | | 29(2) | 146(9) | <i>E,A,A_\pi</i> |
| 777.90 ^a | $\frac{9}{2}^+, \frac{7}{2}^+$ | 777.90 | $\frac{9}{2}^+$ | 0.00 | 51 | | 20(5) | -77(42) | <i>E,A</i> |
| 785.10 | $\frac{5}{2}^+$ | 569.28 | $\frac{7}{2}^+$ | 215.81 | 409 | | -4(2) | -152(6) | <i>E,A</i> |
| | | 460.55 | $\frac{5}{2}^+$ | 324.44 | 58 | | 9(3) | -177(13) | <i>E,A</i> |
| | | 785.02 | $\frac{9}{2}^+$ | 0.00 | 46 | | 3(9) | -112(27) | |
| 832.71 | $\frac{11}{2}^+$ | 832.71 | $\frac{9}{2}^+$ | 0.00 | 367 | | 37(3) | 64(6) | <i>E,A,A_\pi</i> |
| | | 617.17 | $\frac{7}{2}^+$ | 215.81 | 39 | 154 | | | |
| 855.38 | $\frac{7}{2}^+$ | 855.38 | $\frac{9}{2}^+$ | 0.00 | 360 | 32 | -5(2) | -95(3) | <i>E,A</i> |
| | | 639.60 | $\frac{7}{2}^+$ | 215.81 | 72 | | -5(6) | -65(10) | <i>E,A_\pi</i> |
| | | 530.90 | $\frac{5}{2}^+$ | 324.44 | 20 | 28 | | | |
| 861.75 | $\frac{9}{2}^+$ | 861.75 | $\frac{9}{2}^+$ | 0.00 | 282 | | 14(2) | 0(4) | <i>E,A,A_\pi</i> |
| | | 645.78 | $\frac{7}{2}^+$ | 215.81 | 39 | 171 | | | |
| 939.87 | $\frac{1}{2}^+, (\frac{3}{2}^-)$ | 843.27 | $\frac{1}{2}^-$ | 96.60 | 193 | | 3(3) | -172(4) | <i>A</i> |
| | | 615.52 | $\frac{3}{2}^+$ | 324.44 | 92 | 56 | | | |
| 946.79 | $\frac{3}{2}^-$ | 850.19 | $\frac{1}{2}^-$ | 96.60 | 208 | | -4(4) | -117(5) | <i>E,A</i> |
| | | 366.69 | $\frac{3}{2}^-$ | 580.13 | 60 | | 6(4) | -122(7) | <i>E,A</i> |
| | | 289.8 ^b | $\frac{3}{2}^-$ | 656.89 | 8 | | 9(27) | -60(36) | |
| 969.83 | $\frac{7}{2}^+$ | 754.01 | $\frac{7}{2}^+$ | 215.81 | 202 | 32 | 3(2) | -134(9) | <i>E,A_\pi</i> |
| | | 645.27 | $\frac{5}{2}^+$ | 324.44 | 159 | 52 | -3(3) | -112(8) | <i>E,A_\pi</i> |
| | | 970.6 ^c | $\frac{5}{2}^+$ | 0.00 | 13 | | | | |
| 994.58 | $\frac{3}{2}^+$ | 670.14 | $\frac{3}{2}^+$ | 324.44 | 337 | | 0(2) | -164(4) | <i>A_\pi</i> |
| | | 897.87 | $\frac{1}{2}^-$ | 96.60 | 17 | | | | [9] |
| 1049.02 | $\frac{5}{2}^-$ | 392.13 | $\frac{3}{2}^-$ | 656.89 | 57 | | 9(2) | -76(57) | <i>A</i> |
| | | 724.60 | $\frac{5}{2}^+$ | 324.44 | 54 | 10 | 15(4) | -111(18) | <i>A</i> |
| | | 468.96 | $\frac{3}{2}^-$ | 580.13 | 30 | 17 | 8(10) | | <i>D_\pi</i> |
| 1126.95 | $\frac{11}{2}^+$ | 1126.95 | $\frac{5}{2}^+$ | 0.00 | 128 | | -63(2) | 80(6) | <i>E,A,A_\pi</i> |
| | | 911.24 | $\frac{7}{2}^+$ | 215.81 | 62 | | 30(10) | 129(17) | <i>E,A,A_\pi</i> |
| 1141.22 | $\frac{3}{2}^+, \frac{5}{2}^+$ | 816.78 | $\frac{3}{2}^+$ | 324.44 | 182 | | -2(2) | -167(4) | <i>E</i> |
| | | 356.23 | $\frac{5}{2}^+$ | 785.10 | 58 | | 2(4) | -178(11) | <i>E</i> |
| | | 925.42 | $\frac{3}{2}^+$ | 215.81 | 18 | 28 | | | |
| 1199.62 | $\frac{9}{2}^+$ | 983.81 | $\frac{3}{2}^+$ | 215.81 | 101 | 22 | -38(3) | -6(6) | <i>E,A,A_\pi</i> |
| | | 875.18 | $\frac{5}{2}^+$ | 324.44 | 71 | | 17(3) | 8(13) | <i>E,A,A_\pi</i> |
| | | 421.56 | $\frac{3}{2}^-$ | 777.90 | 14 | 61 | | | |
| | | 366.92 | $\frac{11}{2}^+$ | 832.71 | 10 | 50 | | | |
| 1219.85 | $\frac{7}{2}^+$ | 895.41 | $\frac{5}{2}^+$ | 324.44 | 60 | | -12(3) | -105(19) | <i>E,A</i> |
| | | 1219.96 | $\frac{5}{2}^+$ | 0.00 | 59 | 11 | 6(10) | -96(10) | |
| | | 1004.39 | $\frac{5}{2}^+$ | 215.81 | 22 | 8 | 2(6) | -33(26) | <i>D_\pi</i> |
| 1239.99 | $\frac{5}{2}^-$ | 583.10 | $\frac{3}{2}^-$ | 656.89 | 67 | | 11(4) | -83(22) | <i>E,A</i> |
| | | 659.81 ^b | $\frac{3}{2}^-$ | 580.13 | 30 | 13 | -12(5) | | <i>D</i> |
| | | 1024.20 ^b | $\frac{5}{2}^+$ | 215.81 | 24 | 50 | -6(6) | | <i>D</i> |
| | | 915.64 ^b | $\frac{5}{2}^+$ | 324.44 | 16 | 7 | | | |
| | | 292.83 ^b | $\frac{3}{2}^-$ | 946.79 | 10 | 7 | | | |
| 1274.48 | $\frac{7}{2}^-$ | 617.60 | $\frac{3}{2}^-$ | 656.89 | 151 | 41 | -12(3) | -14(11) | <i>D</i> |
| | | 694.45 ^b | $\frac{3}{2}^-$ | 580.13 | 22 | | 10(12) | 3(23) | <i>E</i> |
| | | 949.9 ^b | $\frac{5}{2}^+$ | 324.44 | 5 | | | | |
| 1277.70 | $\frac{9}{2}^-$ | 620.81 | $\frac{3}{2}^-$ | 656.89 | 274 | 16 | 25(2) | 49(6) | <i>E,A,A_\pi</i> |

TABLE I. (Continued).

| E_i (keV) | I_i^π | E_γ (keV) | I_f^π | E_f (keV) | Intensities ^{97}Tc Other | | A_{22} $\times 100$ | Exc. func. | Data used ^d |
|----------------------|--|----------------------|--------------------------------|----------------|---------------------------------------|-----|--------------------------|---------------|---------------------------|
| | | 422.37 | $\frac{7}{2}^+$ | 855.38 | 31 | 43 | | | |
| | | 1062.18 | $\frac{7}{2}^+$ | 215.81 | 18 | 23 | | | |
| 1310.22 | $\frac{7}{2}^+, \frac{9}{2}^+$ | 1094.40 | $\frac{7}{2}^+$ | 215.81 | 65 | 28 | -24(6) | | D |
| | | 1310.7 ^c | $\frac{9}{2}^+$ | 0.00 | 36 | | 16(11) | -88(19) | E, A_π |
| 1311.97 ^a | | 1096.15 | $\frac{7}{2}^+$ | 215.81 | 24 | 14 | | | |
| 1373.28 ^a | $\frac{3}{2}^-$ | 1276.68 | $\frac{1}{2}^-$ | 96.60 | 64 | | -3(4) | -102(17) | E, A |
| | | 426.41 ^b | $\frac{3}{2}^-$ | 946.79 | 13 | 9 | | | |
| | | 1049.0 ^b | $\frac{5}{2}^+$ | 324.44 | 9 | 19 | | | |
| | | 716.8 ^b | $\frac{5}{2}^-$ | 656.89 | 7 | 13 | | | |
| 1380.07 | $\frac{9}{2}^+$ | 547.36 | $\frac{11}{2}^+$ | 832.71 | 64 | | -10(4) | -36(8) | E, D |
| | | 1164.22 | $\frac{7}{2}^+$ | 215.81 | 62 | 20 | -42(4) | | D |
| 1393.33 | $\frac{13}{2}^+$ | 1393.33 | $\frac{9}{2}^+$ | 0.00 | 97 | | 25(6) | 210(9) | E, A |
| | | 620.63 | $\frac{13}{2}^+$ | 772.65 | 30 | 261 | 21(7) | | D |
| | | 560.48 | $\frac{11}{2}^+$ | 832.71 | 29 | 971 | -28(5) | | D |
| | | 531.23 | $\frac{9}{2}^+$ | 861.75 | 19 | 30 | | | |
| 1400.92 ^a | $\frac{3}{2}^-, \frac{5}{2}^-$ | 820.79 | $\frac{3}{2}^-$ | 580.13 | 42 | | 10(3) | -80(14) | E, A, A_π |
| 1409.82 | $\frac{7}{2}^+$ | 1194.01 | $\frac{7}{2}^+$ | 215.81 | 39 | 13 | 6(4) | | D_π |
| | | 1085.25 ^b | $\frac{5}{2}^+$ | 324.44 | 21 | | -19(9) | -66(22) | E, A |
| | | 752.6 ^b | $\frac{5}{2}^-$ | 656.89 | 13 | 221 | | | |
| 1471.35 ^a | $\frac{9}{2}^+, (\frac{7}{2}^+)$ | 1471.35 | $\frac{9}{2}^+$ | 0.00 | 78 | | 19(7) | -48(19) | E, A |
| | | 609.18 | $\frac{13}{2}^+$ | 861.75 | 33 | 15 | 11(7) | | D_π |
| | | 615.66 | $\frac{7}{2}^+$ | 855.38 | 14 | 134 | 22(10) | | D_π |
| | | 1255.56 | $\frac{7}{2}^+$ | 215.81 | 10 | 21 | | | |
| 1512.26 | $\frac{5}{2}$ | 1187.81 | $\frac{5}{2}^+$ | 324.44 | 45 | | 4(8) | -80(12) | E, A |
| | | 855.27 ^b | $\frac{5}{2}^-$ | 656.89 | 32 | 360 | 6(4) | | D |
| | | 1295.8 ^b | $\frac{7}{2}^+$ | 215.81 | 8 | 6 | | | |
| 1518.31 | $\frac{5}{2}^-$ | 938.18 | $\frac{3}{2}^-$ | 580.13 | 43 | 88 | -21(3) | | D, D_π |
| | | 1421.69 ^c | $\frac{1}{2}^-$ | 96.60 | 18 | 9 | | | |
| | | 1194.2 ^b | $\frac{5}{2}^+$ | 324.44 | 7 | 45 | | | |
| 1523.39 | $\frac{7}{2}^+$ | 1198.95 | $\frac{5}{2}^+$ | 324.44 | 70 | | -24(6) | -44(14) | E, D, D_π |
| | | 1307.37 | $\frac{7}{2}^+$ | 215.81 | 12 | 7 | -15(5) | | D_π |
| 1527.3 ^a | | 1202.8 | $\frac{5}{2}^+$ | 324.44 | 9 | 23 | | | |
| 1537.93 ^a | $\frac{11}{2}^+, \frac{13}{2}^+$ | 765.28 | $\frac{13}{2}^+$ | 772.65 | 35 | 17 | -4(11) | | D |
| | | 1538.1 ^c | $\frac{9}{2}^+$ | 0.00 | 28 | 45 | | | |
| 1579.99 | $\frac{5}{2}$ | 923.20 | $\frac{5}{2}^-$ | 656.89 | 23 | 16 | | | |
| | | 999.65 ^b | $\frac{3}{2}^-$ | 580.13 | 20 | 14 | -19(5) | | D |
| | | 1255.46 ^b | $\frac{5}{2}^+$ | 324.44 | 15 | 16 | | | |
| | | 1363.99 ^b | $\frac{7}{2}^+$ | 215.81 | 12 | | | | |
| 1581.46 ^a | $\frac{11}{2}^+, \frac{13}{2}^+, \frac{15}{2}^+$ | 748.75 | $\frac{11}{2}^+$ | 832.71 | 38 | | 32(7) | 145(28) | E, A |
| | | 808.70 ^b | $\frac{13}{2}^+$ | 772.65 | 36 | | 37(4) | 90(20) | E, A |
| 1581.95 ^a | $(\frac{3}{2}, \frac{5}{2}, \frac{7}{2})$ | 925.16 | $\frac{5}{2}^-$ | 656.89 | 45 | 25 | | | |
| | | 1257.96 ^b | $\frac{5}{2}^+$ | 324.44 | 15 | 16 | | | |
| | | 1366.2 ^b | $\frac{7}{2}^+$ | 215.81 | 7 | | | | |
| 1585.8 ^a | $(\frac{7}{2}^+)$ | 1261.3 | $\frac{5}{2}^+$ | 324.44 | 6 | 20 | -25(16) | | D |
| 1625.02 ^a | | 483.79 | $\frac{3}{2}^+, \frac{5}{2}^+$ | 1141.22 | 31 | 686 | | | |
| | | 685.61 ^b | $\frac{1}{2}^+, \frac{3}{2}^-$ | 939.87 | 19 | 15 | | | |
| 1650.19 | $\frac{5}{2}^+, \frac{7}{2}^+$ | 680.36 | $\frac{1}{2}^+, \frac{7}{2}^+$ | 969.83 | 45 | 263 | -4(8) | | D_π |
| | | 794.86 ^b | $\frac{7}{2}^+$ | 855.38 | 18 | | -4(8) | -125(22) | E, D_π |
| | | 1325.6 ^b | $\frac{5}{2}^+$ | 324.44 | 6 | 14 | | | |
| 1654.33 | $\frac{17}{2}^+$ | 881.68 | $\frac{13}{2}^+$ | 772.65 | 105 | | 34(4) | 376(16) | E, A, A_π |
| 1677.69 | $\frac{1}{2}^-, \frac{3}{2}^-, \frac{5}{2}^-$ | 1097.55 | $\frac{3}{2}^-$ | 580.13 | 21 | 16 | -5(5) | | D |
| | | 1020.6 ^b | $\frac{5}{2}^-$ | 656.89 | 9 | 8 | | | |
| 1685.36 | $\frac{15}{2}^+(+)$ | 852.65 | $\frac{11}{2}^+$ | 832.71 | 39 | 18 | 25(7) | | N |
| | | 912.62 ^b | $\frac{13}{2}^+$ | 772.65 | 37 | 44 | 0(0) | | |

TABLE I. (Continued).

| E_i (keV) | I_i^π | E_γ (keV) | I_f^π | E_f (keV) | Intensities | | A_{22} $\times 100$ | Exc. func. | Data used ^d |
|----------------------|---|----------------------|----------------------------------|----------------|------------------|-------|--------------------------|---------------|---------------------------|
| | | | | | ^{97}Tc | Other | | | |
| 1690.12 ^a | $\frac{5}{2}^+, \frac{7}{2}^+$ | 1474.31 | $\frac{7}{2}^+$ | 215.81 | 27 | 10 | -8(5) | -126(13) | E, D |
| 1693.12 | $\frac{5}{2}^+, \frac{7}{2}^+$ | 1477.31 | $\frac{7}{2}^+$ | 215.81 | 33 | 12 | -3(5) | -190(40) | E, D |
| | | 1368.5 ^b | $\frac{5}{2}^+$ | 324.44 | 9 | 15 | | | |
| 1697.9 ^a | | 1482.1 | $\frac{7}{2}^+$ | 215.81 | 10 | 20 | | | |
| 1706.83 ^a | | 429.13 | $\frac{9}{2}^-$ | 1277.70 | 26 | 5 | 21(6) | | |
| 1707.45 | | 1383.01 | $\frac{5}{2}^+$ | 324.44 | 16 | 10 | | | |
| 1720.9 ^a | $\frac{5}{2}^+$ | 726.3 | $\frac{5}{2}^+$ | 994.58 | 14 | | -18(8) | | D |
| 1721.9 | $\frac{5}{2}^+$ | 728.1 | $\frac{5}{2}^+$ | 994.58 | 27 | | | -230(31) | E |
| | | 752.4 ^b | $\frac{7}{2}^+$ | 969.83 | 24 | 210 | -18(6) | | D |
| 1732.97 | $\frac{5}{2}^+(+)$ | 1517.16 | $\frac{7}{2}^+$ | 215.81 | 32 | 14 | -4(2) | | D |
| | | 1153.0 ^b | $\frac{9}{2}^-$ | 580.13 | 7 | 5 | | | |
| 1778.6 | | 1562.8 | $\frac{7}{2}^+$ | 215.81 | 10 | 42 | | | |
| | | 993.6 ^b | $\frac{5}{2}^+$ | 785.10 | 9 | 16 | | | |
| 1797.63 | | 1473.55 | $\frac{5}{2}^+$ | 324.44 | 17 | 20 | | | |
| | | 1012.5 ^b | $\frac{5}{2}^+$ | 785.10 | 8 | 11 | | | |
| 1801.25 ^a | | 1476.80 | $\frac{5}{2}^+$ | 324.44 | 14 | 23 | | | |
| 1815.19 | | 615.57 | $\frac{9}{2}^+$ | 1199.62 | 22 | 126 | | | |
| | | 1491.1 ^b | $\frac{5}{2}^+$ | 324.44 | 8 | 19 | | | |
| | | 1599.9 ^b | $\frac{7}{2}^+$ | 215.81 | 6 | 10 | | | |
| 1834.64 | $\frac{13}{2}^-$ | 556.94 | $\frac{9}{2}^-$ | 1277.70 | 65 | 10 | 29(5) | 159(22) | $E, D, D_\pi, [3]$ |
| 1834.89 | $\frac{11}{2}^+, (\frac{9}{2}^+)$ | 363.54 | $\frac{9}{2}^+, (\frac{7}{2}^+)$ | 1471.35 | 22 | | -16(9) | 123(26) | E, A |
| 1841.76 ^a | $\frac{3}{2}^+, (\frac{5}{2}^-)$ | 901.89 | $\frac{1}{2}^+, (\frac{3}{2}^-)$ | 939.87 | 24 | | -18(9) | -202(41) | E, D |
| | | 847.4 ^b | $\frac{3}{2}^+$ | 994.58 | 7 | 24 | | | |
| 1849.56 | $\frac{15}{2}^+$ | 1076.90 | $\frac{13}{2}^+$ | 772.65 | 43 | | -25(5) | 129(18) | $A, [3]$ |
| | | 456.65 ^b | $\frac{13}{2}^+$ | 1393.33 | 23 | 8 | | | |
| 1850.38 | | 1193.49 | $\frac{9}{2}^-$ | 656.89 | 11 | 41 | | | |
| 1858.59 ^a | | 1201.70 | $\frac{9}{2}^-$ | 656.89 | 11 | 22 | | | |
| 1862.31 ^a | | 1537.87 | $\frac{5}{2}^+$ | 324.44 | 35 | 39 | | | |
| 1864.29 | | 1540.39 | $\frac{5}{2}^+$ | 324.44 | 14 | 19 | | | |
| | | 1008.91 ^b | $\frac{7}{2}^+$ | 855.38 | 12 | 28 | | | |
| 1879.2 | $(\frac{17}{2}^+)$ | 1106.5 | $\frac{13}{2}^+$ | 772.65 | 9 | | 42(23) | | A |
| 1892.58 ^a | $\frac{15}{2}^+$ | 1120.24 | $\frac{13}{2}^+$ | 772.65 | 21 | | -4(8) | 221(33) | E, D, D_π |
| | | 765.64 ^b | $\frac{11}{2}^+$ | 1126.95 | 17 | 35 | | | |
| 1895.66 | | 1062.95 | $\frac{7}{2}^+$ | 832.71 | 13 | 28 | | | |
| 1897.50 ^a | $\frac{5}{2}^+, \frac{7}{2}^+, \frac{9}{2}^+$ | 1681.69 | $\frac{7}{2}^+$ | 215.81 | 20 | | -18(9) | | A |
| 1907.00 ^a | | 1134.35 | $\frac{13}{2}^+$ | 772.65 | 23 | 9 | | | |
| 1913.8 | | 1589.4 | $\frac{5}{2}^+$ | 324.44 | 9 | 5 | | | |
| 1919.3 ^a | | 1594.8 | $\frac{5}{2}^+$ | 324.44 | 8 | 11 | | | |
| 1922.5 ^a | | 1265.6 | $\frac{9}{2}^-$ | 656.89 | 6 | 82 | | | |
| 1925.43 | | 1268.54 | $\frac{9}{2}^-$ | 656.89 | 19 | 27 | | | |
| 1940.5 | | 1616.0 | $\frac{5}{2}^+$ | 324.44 | 8 | 6 | | | |
| 1947.54 ^a | | 1623.10 | $\frac{5}{2}^+$ | 324.44 | 22 | 20 | | | |
| 1949.01 | | 1093.69 | $\frac{5}{2}^+$ | 855.38 | 28 | 64 | | | |
| | | 1163.92 ^b | $\frac{5}{2}^+$ | 785.10 | 15 | 67 | | | |
| 1964.38 ^a | | 1024.51 | $\frac{1}{2}^+, \frac{3}{2}^-$ | 939.87 | 13 | 61 | | | |
| | | 1640.1 ^b | $\frac{5}{2}^+$ | 324.44 | 7 | 18 | | | |
| 1976.50 ^a | | 698.81 | $\frac{9}{2}^-$ | 1277.70 | 26 | 13 | | | |
| 1979.2 ^a | | 1146.5 | $\frac{11}{2}^+$ | 832.71 | 9 | | 5(28) | | |
| 1986.8 | | 1329.9 | $\frac{9}{2}^-$ | 656.89 | 6 | 13 | | | |
| | | 1407.4 | $\frac{9}{2}^-$ | 580.13 | 6 | 2 | | | |
| 1992.5 ^a | | 714.8 | $\frac{9}{2}^-$ | 1277.70 | 7 | 13 | | | |
| 1994.0 | | 1024.2 | $\frac{5}{2}^+, \frac{7}{2}^+$ | 969.83 | 9 | 65 | | | |
| 2001.8 | | 1421.7 | $\frac{9}{2}^-$ | 580.13 | 9 | 18 | | | |
| 2004.10 ^a | | 1009.52 | $\frac{5}{2}^+$ | 994.58 | 20 | 19 | | | |

TABLE I. (*Continued*).

| E_i (keV) | I_i^π | E_γ (keV) | I_f^π | E_f (keV) | Intensities | | A_{22} $\times 100$ | Exc. func. | Data used ^d |
|----------------------|--------------------------------|----------------------|----------------------------------|----------------|------------------|-------|--------------------------|---------------|---------------------------|
| | | | | | ⁹⁷ Tc | Other | | | |
| 2032.88 ^a | | 1171.13 | $\frac{13}{2}^+$ | 861.75 | 11 | 5 | | | |
| 2035.6 | | 1378.8 | $\frac{5}{2}^-$ | 656.89 | 8 | 12 | | | |
| 2048.37 ^a | | 1053.78 | $\frac{3}{2}^+$ | 994.58 | 12 | 27 | | | |
| 2054.74 ^a | | 400.41 | $\frac{17}{2}^+$ | 1654.33 | 10 | | -7(21) | | |
| 2056.1 ^a | | 1283.4 | $\frac{13}{2}^+$ | 772.65 | 9 | 7 | | | |
| 2059.5 | | 1197.8 | $\frac{13}{2}^+$ | 861.75 | 6 | 64 | | | |
| 2067.1 ^a | | 657.3 | $\frac{7}{2}^+$ | 1409.82 | 5 | 115 | | | |
| 2068.99 | $\frac{7}{2}^-, \frac{9}{2}^-$ | 1412.11 | $\frac{5}{2}^-$ | 656.89 | 16 | | 30(38) | <i>E</i> | |
| 2095.6 ^a | | 1240.2 | $\frac{7}{2}^+$ | 855.38 | 8 | 4 | | | |
| | | 1101.4 ^b | $\frac{3}{2}^+$ | 994.58 | 7 | 9 | | | |
| | | | $\frac{5}{2}^-$ | | | | | | |
| 2098.0 ^a | | 823.5 | $\frac{7}{2}^-$ | 1274.48 | 8 | 17 | | | |
| 2117.2 ^a | | 1537.1 | $\frac{3}{2}^-$ | 580.13 | 7 | 66 | | | |
| | | 1255.9 ^b | $\frac{13}{2}^+$ | 861.75 | 5 | 26 | | | |
| 2119.65 ^a | | 1539.51 | $\frac{3}{2}^-$ | 580.13 | 11 | 63 | | | |
| 2121.44 | $(\frac{17}{2}^+)$ | 467.18 | $\frac{17}{2}^+$ | 1654.33 | 10 | 36 | | | |
| | | 1348.79 ^b | $\frac{13}{2}^+$ | 772.65 | 10 | | 50(19) | | <i>A</i> |
| 2130.6 ^a | | 1160.8 | $\frac{5}{2}^+, \frac{7}{2}^+$ | 969.83 | 6 | 11 | | | |
| 2134.8 ^a | | 1362.1 | $\frac{13}{2}^+$ | 772.65 | 8 | 13 | | | |
| 2149.07 | | 1492.18 | $\frac{5}{2}^-$ | 656.89 | 12 | 15 | | | |
| 2257.2 | | 1677.1 | $\frac{3}{2}^-$ | 580.13 | 5 | 6 | | | |
| 2257.75 ^a | | 980.05 | $\frac{9}{2}^-$ | 1277.70 | 11 | 11 | | | |
| 2264.39 ^a | | 1294.56 | $\frac{5}{2}^+, \frac{7}{2}^+$ | 969.83 | 7 | 7 | | | |
| 2331.1 | | 676.8 | $\frac{17}{2}^+$ | 1654.33 | 6 | 18 | | | |
| 2337.6 | $\frac{17}{2}^-$ | 503.0 | $\frac{13}{2}^-$ | 1834.64 | 5 | 4 | | | <i>N</i> |
| | | 487.6 ^b | $\frac{15}{2}^+$ | 1849.56 | 5 | | | | |
| | | | $\frac{7}{2}^-$ | | | | | | |
| 2417.5 ^a | | 1143.0 | $\frac{7}{2}^-$ | 1274.48 | 5 | 2 | | | |
| 2446.6 ^a | | 612.0 | $\frac{13}{2}^-$ | 1834.64 | 6 | 28 | | | |
| 2449.2 ^a | | 911.2 | $\frac{11}{2}^+, \frac{13}{2}^+$ | 1537.93 | 6 | 75 | | | |
| 2533.5 | | 879.1 | $\frac{17}{2}^+$ | 1654.33 | 6 | 41 | | | |

^aNew states observed in this experiment.

^bPlaced in ⁹⁷Tc by coincidence with following γ rays, but assigned to this state on the basis of energy agreement.

^cPlaced between known states by energy agreement alone.

^d*N* means that the NDS [10] spin and parity assignment was used. *E*, *A*, or *D* mean that the excitation function, angular distribution, or DCO, respectively, was used in the spin and parity assignment. A “ π ” subscript is added to *A* or *D* when the measurement excludes parity change for the γ transition.

was the same as that used by Smith and Rickey [6] for Pd nuclei. The calculation of electromagnetic transition properties was the same as that used by Popli [16] for Ag nuclei. This specific model utilizes a rotational Hamiltonian in the strong coupling limit, modified to include a variable moment of inertia (VMI) [17]. The basis states are thus rotational states built on Nilsson single-particle states [15], characterized by good K and Ω , the projections of the total angular momentum \vec{I} and the particle angular momentum \vec{j} , respectively, on the symmetry axis. Pairing is treated by the BCS formalism. The Coriolis and recoil terms, which mix these states, are treated to all order. We would like to emphasize that this basic model has been used for years to interpret strongly deformed nuclei. Aside from differences in inertial quantities, the only deviations of its predictions from familiar rotational patterns are due to the role of the Coriolis interaction.

The predictions of the model fall between two extremes,

TABLE II. Excitation function slope intervals for spin assignment.

| Spin | Slope interval | | | |
|----------------|-----------------|------|-----------------|------|
| | Positive parity | | Negative parity | |
| | Min. | Max. | Min. | Max. |
| $\frac{1}{2}$ | | -295 | | -140 |
| $\frac{3}{2}$ | -295 | -205 | -140 | -86 |
| $\frac{5}{2}$ | -205 | -125 | -86 | -32 |
| $\frac{7}{2}$ | -125 | -40 | -32 | +22 |
| $\frac{9}{2}$ | -40 | +45 | +22 | +76 |
| $\frac{11}{2}$ | +45 | +130 | +76 | +130 |
| $\frac{13}{2}$ | +130 | +215 | +130 | +184 |
| $\frac{15}{2}$ | +215 | +300 | +184 | |
| $\frac{17}{2}$ | +300 | +385 | | |
| $\frac{19}{2}$ | +385 | | | |

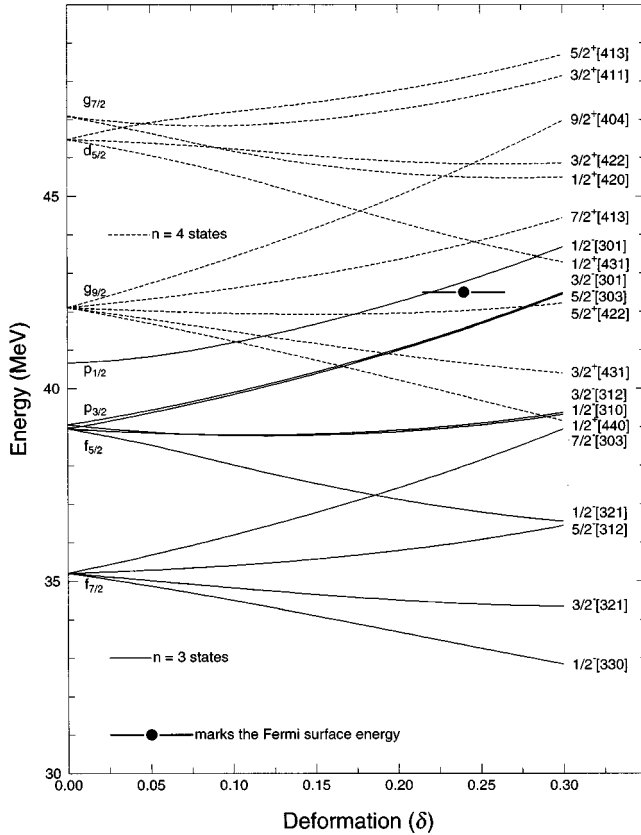


FIG. 6. Nilsson diagram for odd protons in ^{97}Tc .

which depend on the strength of the Coriolis interaction. When Coriolis mixing is small, the features of the basis, namely rotational bands built on states of good Ω , are retained. This limit is approached not only when the deformation is high, but when low values of \vec{j} are involved, or when $j \approx \Omega$. As Coriolis mixing increases, the odd particle tends to become decoupled from the rotating core. If the effects of the Coriolis interaction become large enough, the second limit is approached, in which R , the angular momentum of the core, and j are good quantum numbers rather than Ω . Thus the rotational predictions resemble particle-core multiplets rather than bands. This limit is most commonly realized in slightly deformed nuclei for states with a high, unique value of j . In ^{97}Tc , this might correspond to states of $g_{9/2}$ parentage. The determination of where observed states lie between these two limits is in effect a good assessment of the nuclear deformation.

There are no published $B(E2)$ values for ^{97}Tc to assist in selecting a deformation for the calculation. Our first calculation utilized a deformation of $\delta = 0.18$. Many features of the decay scheme could not be explained at this or smaller deformations, hence calculations at larger deformations were evaluated. Substantial evidence for the sudden onset of large deformations ($\delta = 0.3-0.5$) in a nearby region of the periodic table (Sr, Y) has been reported [5]. The same conditions to which these large deformations were attributed exist in Tc nuclei. A deformation of $\delta = 0.24$ was inferred from observed features. First, the $1/2^+$ state at 939.87 keV could not be explained by the model at lower deformations. The domi-

TABLE III. Parameters used in the calculation.

| Shell number | κ | μ | μ_2 | λ (MeV) | Δ (MeV) | Atten. factor |
|--------------|----------|-------|---------|-----------------|----------------|---------------|
| 4 | 0.062 | 0.45 | 0.43 | 41.94 | 1.5 | 0.85 |
| 3 | 0.060 | 0.52 | 0.52 | 42.50 | 1.5 | 0.8 |

nant decay observed was by an $E1$ transition to the $1/2^-$ state at 96.60 keV. This is inconsistent with the decay of any state with $g_{9/2}$ parentage, since the $1/2^-$ state must have $p_{1/2}$ or $p_{3/2}$ parentage. At the higher deformation the $1/2^+$ [431] Nilsson state lies at an appropriate energy to explain the origin of the observed state. This Nilsson state has sizable components with $s_{1/2}$, $d_{3/2}$, and $d_{5/2}$ parentage, and the calculated $E1$ decay is not only allowed, but dominant. Second, at lower deformations the predicted branching ratios for the decay of several low-lying positive-parity states to the lowest $9/2^+$ and $7/2^+$ states were wrong. For example, the data show that the $5/2^+$ state at 324.44 keV prefers decay to the $9/2^+$ state over the $7/2^+$ state. At a deformation of $\delta = 0.18$, the calculation predicted only a 20% branch to the $9/2^+$ state. At $\delta = 0.24$, this prediction is reversed, with the dominant decay as observed.

This deformation might seem too large in view of the relatively large rotational energies compared to rare-earth and actinide nuclei with similar deformations. However, inertial parameters depend on mass as well as deformation. A crude analysis of inertial parameters for $7/2^+$ states extracted from level schemes [18] established for nuclei in known regions of deformation [19] shows that the average value of $\hbar^2/2\mathcal{J}$ for ^{25}Al ($\delta=0.35$) is roughly 200 keV, for ^{175}Lu ($\delta=0.28$) roughly 13 keV, and for ^{237}Np ($\delta=0.25$) roughly 6 keV. While an extrapolation of these inertial parameters to the $A \approx 100$ is semiquantitative at best, we feel that average values of $\hbar^2/2\mathcal{J}$ extracted from our data (roughly 70–90 keV for the same spin) are consistent with a deformation of $\delta=0.24$.

The parameters used for the Nilsson calculations were chosen to give energies at zero deformation consistent with those tabulated by Reehal and Sorenson [20]. The Fermi energies for positive and negative parities were chosen on the basis of filling Nilsson states with the 43 protons of ^{97}Tc , and then making minor adjustments. The pairing parameter Δ was taken from systematics. Coriolis and recoil terms were attenuated by the same factor. The values of these parameters are given in Table III.

The basis states for the calculation were restricted to the Nilsson states near the Fermi surface. The specific states included in the basis, along with their single-particle energies, are given in Table IV. In general we do not treat the VMI parameters \mathcal{J}_0 and C as free parameters for all basis states, although different sets were adopted for positive- and negative-parity states. In the fine-tuning stage of the calculation, the value of C was changed for 4 of the 16 basis states. The VMI parameters are also given in Table IV.

Table V presents the comparison of experimental and calculated results for ^{97}Tc . This table includes only the experimental states which have been identified on the basis of their energies and branching ratios as corresponding to rotational states predicted by the model. Branching ratios were the ma-

TABLE IV. Basis states and associated parameters used in the calculation.

| State | E_{sp} | \mathcal{J}_0 | C |
|---------------|----------|-----------------|-------|
| $1/2^+$ [420] | 45.497 | 0.0 | 0.075 |
| $1/2^+$ [431] | 43.876 | 0.0 | 0.100 |
| $1/2^+$ [440] | 39.792 | 0.0 | 0.075 |
| $1/2^+$ [411] | 47.548 | 0.0 | 0.075 |
| $1/2^+$ [422] | 45.842 | 0.0 | 0.075 |
| $1/2^+$ [431] | 40.655 | 0.0 | 0.075 |
| $1/2^+$ [413] | 48.084 | 0.0 | 0.075 |
| $1/2^+$ [422] | 42.017 | 0.0 | 0.075 |
| $1/2^+$ [413] | 43.736 | 0.0 | 0.045 |
| $1/2^+$ [404] | 45.737 | 0.0 | 0.075 |
| $1/2^-$ [301] | 42.766 | 0.0 | 0.011 |
| $1/2^-$ [310] | 39.005 | 0.0 | 0.011 |
| $1/2^-$ [321] | 36.842 | 0.0 | 0.011 |
| $1/2^-$ [301] | 41.563 | 0.0 | 0.060 |
| $1/2^-$ [312] | 39.051 | 0.0 | 0.011 |
| $1/2^-$ [303] | 41.525 | 0.0 | 0.060 |

major reason for excluding some of the experimental states. For example, consider the second $7/2^+$ state of the calculation, with a calculated energy of 1016 keV. The calculation predicts equal branches to the lowest $5/2^+$ and $7/2^+$ states, and a very small branch to the $9/2^+$ ground state. Three $7/2^+$ states were observed experimentally, at 855.38, 969.83, and 1219.85 keV, which could be candidates for the calculated state on the basis of energy alone. However the 855.38- and 1219.85-keV states have large branches to the ground state and small branches to the lowest $7/2^+$ state, and hence were excluded. As Table V shows, the 969.83-keV state has branching ratios which agree with those calculated. Columns 1 and 2 give the experimental and theoretical energies for each initial state, and column 3 gives the initial spin and parity. If more than one spin was experimentally possible, only the spin agreeing with the theoretical spin is listed and identified with a footnote. (There are seven states in this category.) 9 of the 35 initial states in this table had no experimental spin assignments, but are included because their energies and branching patterns agreed with those calculated. Values of I^π inferred from the model calculations are enclosed in double parentheses. The model identification of the initial state is given in column 8. In the calculation we considered decay probabilities to all final states to which transitions were possible on the basis of energies and spin changes. However, because of space limitations, the table only includes branches which were either observed or predicted to be observable. For the branches included, column 4 gives the final spin and parity and column 5 the γ -ray energy. Columns 6 and 7 give the experimental and theoretical branching ratios, and column 9 gives the model identification for each final state.

Three negative-parity ‘‘bands’’ have been identified, with bandheads $1/2^-$, $3/2^-$, and $5/2^-$. These three bands, along with the predicted energies, are shown in Fig. 7. Coriolis mixing is small because of the low values of j that contribute to the wave functions. The calculated wave functions for members of the $1/2^-$ band are better than 96% $1/2^-$ [301], so

that the result is an essentially pure Nilsson band. The Coriolis interaction has caused some mixing for the $3/2^-$ and $5/2^-$ bands, although a single Nilsson component dominates each state. Members of the $3/2^-$ band are better than 73% $3/2^-$ [301], and members of the $5/2^-$ band are better than 73% $5/2^-$ [303]. Thus Table V identifies the bands as $1/2^-$ [301], $3/2^-$ [301], and $5/2^-$ [303], respectively. States in the $3/2^-$ and $5/2^-$ bands decay in a manner which might seem uncharacteristic of rotational bands, in that the dominant decay modes for members of both bands are $M1$ transitions to members of the $1/2^-$ band rather than intraband transitions. In our model the physics responsible for the dominance of the interband $M1$ transitions is quite simple. For pure Nilsson bands, with no Coriolis mixing, transition probabilities for interband $M1$ transitions between $3/2^-$ [301] and $1/2^-$ [301] bands are very large since they are spin-flip transitions, typically 20–100 times larger than calculated intraband $M1$ transitions in pure $3/2^-$ [301] or $5/2^-$ [303] bands. The component of $3/2^-$ [301] in the $5/2^-$ band due to Coriolis mixing is enough to cause members of the $5/2^-$ band to decay predominantly to members of the $1/2^-$ band. In most cases the calculation reproduces experimental branching ratios very well. The decay of the 1049.02-, 1274.48-, and 1581.95-keV states seen in Table V are examples of this agreement. The 1049.02- and 1581.95-keV states decay predominantly by interband transitions, as the calculation predicts. The 1274.48-keV state decays predominantly by intraband transitions, in agreement with the calculation.

There are a few cases where the agreement is not as good. The poorest agreement occurs for states with excitation energies greater than 1900 keV, which were observed to decay by single transitions with small intensities near our detection limit. The theoretical state with the best energy match for a particular observed state may have several appreciable branches. We have made associations with theoretical predictions for these states if the calculation predicts a large branch for the experimentally observed transition, since other branches might not be detectable. We have included all the theoretical branches in Table V. Some of these associations may not be correct, but we feel that this does not detract from the overall reliability of the model associations.

In Table V a positive-parity band with a bandhead spin of $1/2^+$ has also been identified. The calculation associates this band with a relatively pure $1/2^+$ [431] Nilsson band, ranging from 70% at low spins to 50% at higher spins. This band, along with predicted energies, is also shown in Fig. 7. The increase in Coriolis mixing over that for the negative-parity bands is due to components of higher values of j in the wave functions. However, the Coriolis mixing is still small enough so that no dominant j prevails. The decay of the $1/2^+$ bandhead is unusual in that the dominant branch is an $E1$ transition to the $1/2^-$ state at 96.5 keV. The calculation agrees with this, as was discussed earlier. At smaller deformations this $E1$ branch could not be reproduced.

The calculated wave functions for the remaining positive-parity states included in Table V show substantial Coriolis mixing, even though the deformation is the same as for the other states described above. The model associates these states with Nilsson states of predominantly $g_{9/2}$ parentage. However, the calculated results deviate appreciably from the

TABLE V. Comparison of experimental and calculated results for ^{97}Tc . I^π values enclosed in double parentheses are inferred from model comparisons alone, since there was no experimental assignment.

| Expt. (keV) | E_i Theor. (keV) | I_i^π | I_f^π | E_γ (keV) | Branching ratio | | Theoretical identification | |
|-------------|-----------------------|---------------------|------------------|---------------------|-----------------|--------|----------------------------|-----------------------|
| | | | | | Expt. | Theor. | Initial state | Final state |
| 0 | | $\frac{9}{2}^+$ | | | | | $g_{9/2}, R=0$ | |
| 96.5 | 97 | $\frac{1}{2}^-$ | $\frac{9}{2}^+$ | 96.50 | 1.00 | 1.00 | $\frac{1}{2}^- [301]$ | $g_{9/2}, R=0$ |
| 215.81 | 39 | $\frac{7}{2}^+$ | $\frac{9}{2}^+$ | 215.81 | 1.00 | 1.00 | $g_{9/2}, R=2$ | $g_{9/2}, R=0$ |
| 324.44 | 54 | $\frac{5}{2}^+$ | $\frac{9}{2}^+$ | 324.44 | 0.99 | 0.67 | $g_{9/2}, R=2$ | $g_{9/2}, R=0$ |
| | | | $\frac{7}{2}^+$ | 109.16 | 0.01 | 0.33 | | $g_{9/2}, R=2$ |
| 580.13 | 436 | $\frac{3}{2}^-$ | $\frac{1}{2}^-$ | 483.53 | 1.00 | 1.00 | $\frac{1}{2}^- [301]$ | $\frac{1}{2}^- [301]$ |
| 656.89 | 514 | $\frac{5}{2}^-$ | $\frac{1}{2}^-$ | 560.29 | 0.98 | 0.98 | $\frac{1}{2}^- [301]$ | $\frac{1}{2}^- [301]$ |
| | | | $\frac{3}{2}^+$ | 332.39 | 0.01 | 0.00 | | $g_{9/2}, R=2$ |
| | | | $\frac{1}{2}^+$ | 441.0 | 0.01 | 0.00 | | $g_{9/2}, R=2$ |
| | | | $\frac{3}{2}^-$ | 76.75 | 0.00 | 0.02 | | $\frac{1}{2}^- [301]$ |
| 772.65 | 742 | $\frac{13}{2}^+$ | $\frac{5}{2}^+$ | 772.65 | 1.00 | 1.00 | $g_{9/2}, R=2$ | $g_{9/2}, R=0$ |
| 785.10 | 963 | $\frac{5}{2}^+$ | $\frac{5}{2}^+$ | 569.28 | 0.80 | 0.86 | $g_{9/2}, R=2,4$ | $g_{9/2}, R=2$ |
| | | | $\frac{3}{2}^+$ | 460.55 | 0.11 | 0.13 | | $g_{9/2}, R=2$ |
| | | | $\frac{1}{2}^+$ | 785.02 | 0.01 | 0.01 | | $g_{9/2}, R=0$ |
| 832.71 | 532 | $\frac{11}{2}^+$ | $\frac{3}{2}^+$ | 832.71 | 0.91 | 0.86 | $g_{9/2}, R=2,4$ | $g_{9/2}, R=0$ |
| | | | $\frac{1}{2}^+$ | 617.17 | 0.09 | 0.14 | | $g_{9/2}, R=2$ |
| 939.87 | 885 | $\frac{1}{2}^+$ a | $\frac{1}{2}^-$ | 843.27 | 0.68 | 0.91 | $\frac{1}{2}^+ [431]$ | $\frac{1}{2}^- [301]$ |
| | | | $\frac{3}{2}^+$ | 615.52 | 0.32 | 0.09 | | $g_{9/2}, R=2$ |
| 946.79 | 775 | $\frac{3}{2}^-$ | $\frac{1}{2}^-$ | 850.19 | 0.78 | 0.87 | $\frac{3}{2}^- [301]$ | $\frac{1}{2}^- [301]$ |
| | | | $\frac{1}{2}^-$ | 366.69 | 0.19 | 0.11 | | $\frac{1}{2}^- [301]$ |
| | | | $\frac{1}{2}^-$ | 289.85 | 0.03 | 0.02 | | $\frac{1}{2}^- [301]$ |
| 969.83 | 1016 | $\frac{7}{2}^+$ | $\frac{3}{2}^+$ | 754.01 | 0.54 | 0.38 | $g_{9/2}, R=2,4$ | $g_{9/2}, R=2$ |
| | | | $\frac{1}{2}^+$ | 645.27 | 0.42 | 0.37 | | $g_{9/2}, R=2$ |
| | | | $\frac{3}{2}^+$ | 970.6 | 0.22 | 0.04 | | $g_{9/2}, R=0$ |
| 994.58 | 868 | $\frac{3}{2}^+$ | $\frac{1}{2}^-$ | 670.14 | 0.95 | 0.85 | $\frac{1}{2}^+ [431]$ | $g_{9/2}, R=2$ |
| | | | $\frac{1}{2}^-$ | 897.87 | 0.05 | 0.02 | | $\frac{1}{2}^- [301]$ |
| 1049.02 | 902 | $\frac{5}{2}^-$ | $\frac{1}{2}^-$ | 392.13 | 0.40 | 0.46 | $\frac{3}{2}^- [301]$ | $\frac{1}{2}^- [301]$ |
| | | | $\frac{3}{2}^+$ | 724.60 | 0.39 | 0.04 | | $g_{9/2}, R=2$ |
| | | | $\frac{1}{2}^-$ | 468.96 | 0.21 | 0.48 | | $\frac{1}{2}^- [301]$ |
| 1141.22 | 1063 | $\frac{3}{2}^+$ a | $\frac{3}{2}^+$ | 816.78 | 0.70 | 0.80 | $g_{9/2}, R=2,4$ | $g_{9/2}, R=2$ |
| | | | $\frac{1}{2}^+$ | 356.23 | 0.23 | 0.14 | | $g_{9/2}, R=2,4$ |
| | | | $\frac{3}{2}^+$ | 925.42 | 0.07 | 0.06 | | $g_{9/2}, R=2$ |
| 1239.99 | 1272 | $\frac{5}{2}^-$ | $\frac{1}{2}^-$ | 583.10 | 0.46 | 0.52 | $\frac{5}{2}^- [303]$ | $\frac{1}{2}^- [301]$ |
| | | | $\frac{1}{2}^-$ | 659.81 | 0.20 | 0.42 | | $\frac{1}{2}^- [301]$ |
| | | | $\frac{3}{2}^+$ | 1024.20 | 0.16 | 0.00 | | $g_{9/2}, R=2$ |
| | | | $\frac{1}{2}^+$ | 915.64 | 0.11 | 0.00 | | $g_{9/2}, R=2$ |
| | | | $\frac{3}{2}^-$ | 292.83 | 0.07 | 0.05 | | $\frac{3}{2}^- [301]$ |
| 1274.48 | 1072 | $\frac{7}{2}^-$ | $\frac{1}{2}^-$ | 617.60 | 0.85 | 0.82 | $\frac{1}{2}^- [301]$ | $\frac{1}{2}^- [301]$ |
| | | | $\frac{1}{2}^-$ | 694.45 | 0.12 | 0.18 | | $\frac{1}{2}^- [301]$ |
| | | | $\frac{3}{2}^+$ | 949.93 | 0.03 | 0.00 | | $g_{9/2}, R=2$ |
| 1277.70 | 1205 | $\frac{9}{2}^-$ | $\frac{1}{2}^-$ | 620.81 | 0.82 | 1.00 | $\frac{1}{2}^- [301]$ | $\frac{1}{2}^- [301]$ |
| | | | $\frac{3}{2}^+$ | 422.37 | 0.09 | 0.00 | | $g_{9/2}, R=2,4$ |
| | | | $\frac{1}{2}^+$ | 1062.18 | 0.05 | 0.00 | | $g_{9/2}, R=2$ |
| 1310.22 | 1007 | $\frac{9}{2}^+$ a | $\frac{3}{2}^+$ | 1094.40 | 0.64 | 0.67 | $g_{9/2}, R=2,4$ | $g_{9/2}, R=2$ |
| | | | $\frac{1}{2}^+$ | 1310.7 | 0.36 | 0.15 | | $g_{9/2}, R=0$ |
| 1311.97 | 1259 | $((\frac{5}{2}^+))$ | $\frac{1}{2}^+$ | 1096.15 | 1.00 | 0.85 | $\frac{1}{2}^+ [431]$ | $g_{9/2}, R=2$ |
| 1471.35 | 1320 | $\frac{7}{2}^+$ a | $\frac{1}{2}^+$ | 1471.35 | 0.89 | 0.79 | $\frac{1}{2}^+ [431]$ | $g_{9/2}, R=0$ |
| | | | $\frac{3}{2}^+$ | 1255.56 | 0.11 | 0.06 | | $g_{9/2}, R=2$ |
| 1581.46 | 1579 | $\frac{15}{2}^+$ a | $\frac{11}{2}^+$ | 748.75 | 0.52 | 0.38 | $g_{9/2}, R=4$ | $g_{9/2}, R=2,4$ |
| | | | $\frac{13}{2}^+$ | 808.70 | 0.48 | 0.62 | | $g_{9/2}, R=2$ |
| 1581.95 | 1424 | $(\frac{7}{2}^-)$ a | $\frac{1}{2}^-$ | 925.16 | 0.67 | 0.67 | $\frac{5}{2}^- [303]$ | $\frac{1}{2}^- [301]$ |
| | | | $\frac{3}{2}^+$ | 1257.96 | 0.22 | 0.15 | | $g_{9/2}, R=2$ |

TABLE V. (Continued).

| E_i | | I_i^π | I_f^π | E_γ (keV) | Branching ratio | | Theoretical identification | |
|----------------|-----------------|------------------------------|---|---|--------------------------------------|--------------------------------------|--|----------------|
| Expt. (keV) | Theor. (keV) | | | | Expt. | Theor. | Initial state | Final state |
| 1625.02 | 1590 | $((\frac{1}{2}^+))$ | $\frac{7}{2}^+$ $\frac{3}{2}^+$ $\frac{1}{2}^+$ $\frac{5}{2}^+$ $\frac{3}{2}^+$ | 1366.2 483.79 685.61 1300.57 630.44 | 0.10 0.62 0.38 0.00 0.00 | 0.05 0.47 0.06 0.25 0.17 | $g_{9/2}, R=2$ $g_{9/2}, R=4$ $\frac{1}{2}^+[431]$ $g_{9/2}, R=2$ $\frac{1}{2}^+[431]$ | |
| 1654.33 | 1899 | $\frac{17}{2}^+$ | $\frac{13}{2}^+$ | 881.68 | 1.00 | 1.00 | $g_{9/2}, R=4$ $g_{9/2}, R=2$ | |
| 1706.83 | 1894 | $((\frac{11}{2}^-))$ | $\frac{9}{2}^-$ | 429.13 | 1.00 | 1.00 | $\frac{1}{2}^- [301]$ $\frac{1}{2}^- [301]$ | |
| 1834.64 | 2058 | $\frac{13}{2}^-$ | $\frac{9}{2}^-$ | 556.94 | 1.00 | 1.00 | $\frac{1}{2}^- [301]$ $\frac{1}{2}^- [301]$ | |
| 1979.2 | 1927 | $((\frac{13}{2}^+))$ | $\frac{11}{2}^+$ $\frac{13}{2}^+$ | 1146.5 1206.6 | 1.00 0.00 | 0.75 0.25 | $g_{9/2}, R=4,6$ $g_{9/2}, R=2,4$ $g_{9/2}, R=2$ | |
| 1992.5 | 2014 | $((\frac{9}{2}^-))$ | $\frac{9}{2}^-$ $\frac{5}{2}^-$ $\frac{7}{2}^-$ | 714.8 943.5 718.0 | 1.00 0.00 0.00 | 0.36 0.37 0.27 | $\frac{5}{2}^- [303]$ $\frac{1}{2}^- [301]$ $\frac{5}{2}^- [303]$ $\frac{1}{2}^- [301]$ | |
| 1994.0 | 2068 | $((\frac{9}{2}^+))$ | $\frac{7}{2}^+$ $\frac{7}{2}^+$ | 1024.2 1778.2 | 1.00 0.00 | 0.35 0.25 | $\frac{1}{2}^+[431]$ $g_{9/2}, R=2,4$ $g_{9/2}, R=2$ | |
| 2056.1 | 2256 | $((\frac{11}{2}^+))$ | $\frac{13}{2}^+$ | 1283.4 | 1.00 | 0.75 | $\frac{1}{2}^+[431]$ $g_{9/2}, R=2$ | |
| 2068.99 | 1846 | $\frac{7}{2}^-$ ^a | $\frac{5}{2}^-$ | 1412.11 | 1.00 | 0.55 | $\frac{3}{2}^- [301]$ $\frac{1}{2}^- [301]$ | |
| 2257.75 | 2471 | $((\frac{9}{2}^-))$ | $\frac{9}{2}^-$ $\frac{7}{2}^-$ | 980.05 983.27 | 1.00 0.00 | 0.60 0.40 | $\frac{3}{2}^- [301]$ $\frac{1}{2}^- [301]$ | |
| 2264.39 | 2256 | $((\frac{9}{2}^+))$ | $\frac{7}{2}^+$ | 1294.56 | 1.00 | 0.5 | $g_{9/2}, R=4,6$ $g_{9/2}, R=2,4$ | |

^aOther spins are allowed experimentally.

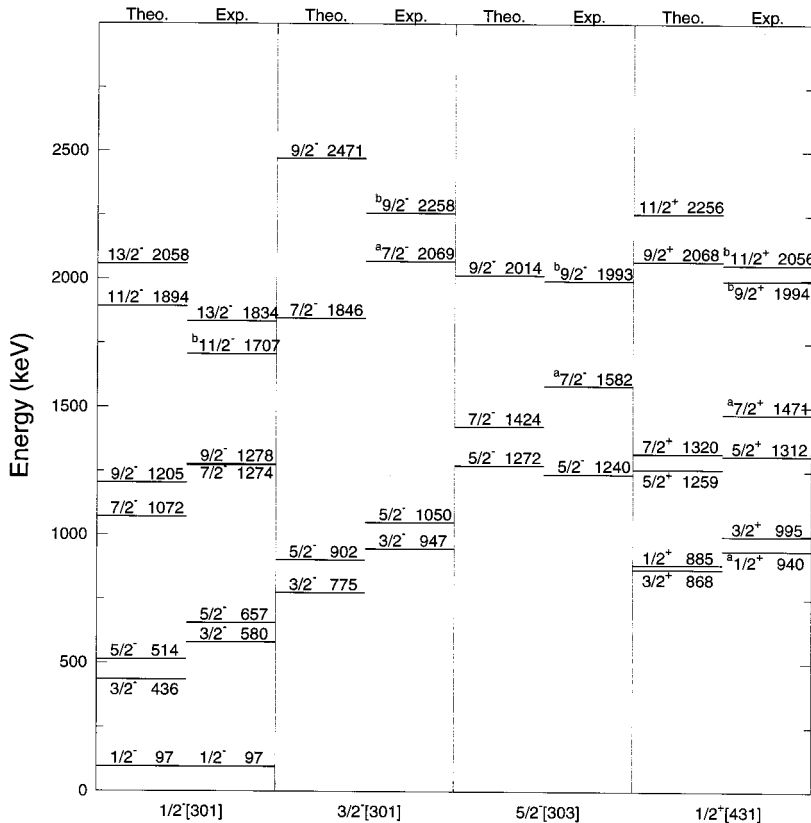


FIG. 7. Band structure identified in ^{97}Tc . The superscript “a” on an experimental spin indicates that the measurement allows for another spin. The superscript “b” indicates that no spin was measured, and the spin shown is from the model association based on energy and branching ratios.

TABLE VI. Summary of calculated wave functions for states of predominantly $g_{9/2}$ parentage. Entries for Nilsson components, j , and R are fractions of total.

| Spin | Nilsson component | | | | | j (9/2) | R | | | |
|--------------------|-------------------|-------|-------|-------|-------|--------------|-------|-------|-------|-------|
| | [440] | [431] | [422] | [413] | [404] | | 0 | 2 | 4 | 6 |
| $(\frac{1}{2})_2$ | 0.79 | | | | | 0.916 | 0.004 | 0.052 | 0.944 | |
| $(\frac{3}{2})_2$ | 0.04 | 0.69 | | | | 0.711 | 0.026 | 0.198 | 0.774 | 0.002 |
| $(\frac{5}{2})_1$ | 0.21 | 0.37 | 0.43 | | | 0.899 | 0.081 | 0.804 | 0.115 | |
| $(\frac{5}{2})_2$ | 0.44 | 0.37 | 0.43 | | | 0.655 | 0.085 | 0.251 | 0.636 | 0.027 |
| $(\frac{7}{2})_1$ | 0.02 | 0.22 | 0.53 | 0.23 | | 0.946 | 0.011 | 0.948 | 0.029 | 0.012 |
| $(\frac{7}{2})_2$ | 0.07 | 0.24 | 0.01 | 0.44 | | 0.619 | 0.094 | 0.258 | 0.644 | 0.001 |
| $(\frac{9}{2})_1$ | 0.17 | 0.29 | 0.37 | 0.16 | 0.01 | 0.938 | 0.797 | 0.140 | 0.053 | 0.010 |
| $(\frac{9}{2})_2$ | 0.34 | 0.12 | 0.06 | 0.41 | 0.06 | 0.919 | 0.014 | 0.533 | 0.441 | 0.008 |
| $(\frac{9}{2})_4$ | 0.14 | 0.01 | 0.28 | 0.12 | 0.18 | 0.837 | 0.120 | 0.116 | 0.305 | 0.448 |
| $(\frac{11}{2})_1$ | 0.02 | 0.21 | 0.46 | 0.28 | 0.02 | 0.957 | | 0.762 | 0.229 | 0.005 |
| $(\frac{11}{2})_2$ | 0.07 | 0.32 | 0.03 | 0.43 | 0.13 | 0.887 | | 0.134 | 0.453 | 0.402 |
| $(\frac{13}{2})_1$ | 0.22 | 0.30 | 0.33 | 0.15 | 0.01 | 0.940 | | 0.900 | 0.057 | 0.041 |
| $(\frac{13}{2})_2$ | 0.34 | 0.10 | 0.08 | 0.42 | 0.07 | 0.930 | | 0.001 | 0.776 | 0.201 |
| $(\frac{15}{2})_1$ | 0.02 | 0.21 | 0.44 | 0.30 | 0.02 | 0.960 | | | 0.883 | 0.103 |
| $(\frac{17}{2})_1$ | 0.22 | 0.30 | 0.30 | 0.15 | 0.01 | 0.941 | | | 0.905 | 0.065 |

multiplet limit. Table VI gives a summary of the model wave functions. (Only the basis states of $g_{9/2}$ parentage are included. The fact that the Nilsson components do not total one for some states indicates components of other basis states.) It is clear that Ω is not a good quantum number. The fraction of $j=9/2$ is high for all states in Table VI. While this is a necessary condition for multiplet states, it may be misleading. The Nilsson states themselves are nearly pure $j=9/2$ states, ranging from 0.79 for the $1/2^+[440]$ state to 1.00 for the $9/2^+[404]$ state. However, many of the wave functions contain more than one sizable value of R . For example, the second $9/2^+$ state shows roughly equal components of $R=2$ and $R=4$. This is in sharp contrast to the less-deformed ^{111}Ag [2], where the $R=2$ component was 0.85. The improved calculated branching ratios for many states of $g_{9/2}$ parentage, such as the 324.44-keV $5/2^+$ state mentioned earlier, are a direct result of the deviation from the multiplet limit at the deformation used in the calculation. Indeed, the observed branching ratio for the corresponding $5/2^+$ state in ^{111}Ag [2] was the opposite of that observed here, in agreement with the calculation at a smaller deformation. In the identification column of Table V, more than one R component is listed if the dominant R component was less than 0.8. Table VI shows a consistent trend for the lowest energy state of a given spin to be a better ‘‘multiplet’’ state, that is, more single-valued in R . The calculated wave functions for the first $9/2^+$ and $7/2^+$ states show why they become the ground and second-excited states. They both have a large $5/2^+[422]$ component, which indicates their origin as low-lying states, but show enough Coriolis mixing to depress their energies below the unperturbed $5/2^+$ bandhead.

There are of course observed states which are not described by this simple particle-rotor model. If one considers ^{96}Mo as the ‘‘core’’ for ^{97}Tc , there are four ‘‘nonrotational’’ excited states known [21] below 2 MeV, 0^+ (1148 keV), 2^+ (1497 keV), 2^+ (1626 keV), and 4^+ (1870 keV). Thus one should expect to find ‘‘nonrotational’’ states in ^{97}Tc which are outside of the model space. The success of the

model in predicting energies and branching ratios for states at low excitation energies suggests that that is little mixing of ‘‘rotational’’ and ‘‘nonrotational’’ states. Of the 16 observed states below 1.0 MeV, 13 are accounted for by the model (all of the states below 750 keV). As the excitation energy increases, there are more unexplained states. Between 1.0 and 1.5 MeV, 8 of the 16 observed states cannot be identified, and likewise for 35 of the 45 observed states between 1.5 and 2.0 MeV.

V. CONCLUSIONS

The present work has extended previously available information on the properties of intermediate-spin states in the low energy region of ^{97}Tc . The $^{96}\text{Mo}(^3\text{He},pn\gamma)^{97}\text{Tc}$ reaction has proven to be effective in populating both yrast and nonyrast states. 45 new levels have been established, which roughly doubles the number of known states below 2 MeV. The use of the proton- γ coincidence system, by reducing background and eliminating photopeaks from competing reaction channels, allowed the quantitative analysis of many weak transitions placed in the level scheme. As a result reliable spin assignments could be established for the majority of states.

The interpretation of the structure of ^{97}Tc in the framework of a rotational model presented in the present work is conceptually different from the vibrational-IBFM interpretation presented in previous work [3]. But the IBFM calculation dealt with states near the yrast line, for which different models can provide similar interpretations. The rotational calculation describes not only the near-yrast states, but much of the new results as well. We believe the rotational calculation, which implicitly tests the hypothesis that ^{97}Tc is deformed, has proven to be successful.

We have attempted to show that the basic features of ^{97}Tc can be explained naturally if it is deformed. While the Coriolis interaction has been shown to play a decided role in the model predictions, its affects have been small enough for

many states to allow the identification of four reasonably pure rotational bands in ^{97}Tc . Coriolis mixing is smallest for the three negative-parity bands identified, although the energies and decay properties are certainly affected. Coriolis mixing is somewhat larger in the positive-parity band identified, but is still small enough to retain its nature as a $1/2^+$ [431] rotational band. The identification of this band at a low excitation energy is a signature of the substantial deformation of ^{97}Tc . Positive-parity states for which $g_{9/2}$ parcentage is deduced exhibit the largest degree of Coriolis mixing. There is no consistent band structure for these states, as the wave functions are shown to contain admixtures of several Nilsson states. However the Coriolis mixing is not large

enough to drive these states to the multiplet limit attributed in a previous work [2] to the structure of similar states in ^{111}Ag . In the present work this decrease in Coriolis mixing is attributed to a larger deformation.

We would like to emphasize that the deformation of $\delta = 0.24$ suggested in the present work for ^{97}Tc is based primarily on the model analysis of electromagnetic transition properties. We feel that the observed branching ratios, and their differences from those observed in ^{111}Ag , are a strong indicator of the deformation of ^{97}Tc .

This work was supported in part by the National Science Foundation.

-
- [1] C. S. Whistnant, K. D. Carnes, R. H. Castain, F. A. Rickey, G. S. Samudra, and P. C. Simms, *Phys. Rev. C* **34**, 443 (1986).
- [2] Sadek Zeghib, F. A. Rickey, G. S. Samudra, P. C. Simms, and Ning Wang, *Phys. Rev. C* **36**, 939 (1987).
- [3] D. Hippe, H. W. Schuh, U. Kaup, K. O. Zell, P. von Brentano, and D. B. Fossan, *Z. Phys. A* **311**, 329 (1983).
- [4] *Interacting Bose-Fermi Systems in Nuclei*, edited by F. Iachello (Plenum, New York, 1981).
- [5] R. F. Petry, J. D. Goulden, F. K. Wahn, John C. Hill, R. L. Gill, and A. Piotrowski, *Phys. Rev. C* **37**, 2704 (1988).
- [6] H. A. Smith, Jr. and F. A. Rickey, *Phys. Rev. C* **14**, 1946 (1976).
- [7] R. A. Mayer, Lawrence Livermore Laboratory, Livermore Report UCRL M-100, 1978.
- [8] B. A. Emelianov, L. P. Kabina, I. A. Kondurov, Yu E. Loginov, and P. A. Sushkov, *Nucl. Instrum. Methods* **178**, 555 (1980).
- [9] B. W. Huber and K. Kramer, *Z. Phys.* **267**, 111 (1974).
- [10] B. Haesner and P. Luksch, *Nucl. Data Sheets* **46**, 607 (1985); A. Artna-Cohen, *ibid.* **70**, 85 (1993).
- [11] W. Zipper, A. Dewald, W. Lieberz, R. Reinhardt, W. Dichter, F. Seiffert, and P. von Brentano, *Nucl. Phys.* **A504**, 36 (1989).
- [12] Jean Kern, Pavel Cejnar, and Wiktor Zipper, *Nucl. Phys.* **A554**, 246 (1993).
- [13] K. S. Krane, R. M. Steffen, and R. M. Wheeler, *Nucl. Data Sect. A* **11**, 351 (1973).
- [14] J. A. Grau, L. E. Samuelson, F. A. Rickey, P. C. Simms, and H. A. Smith, *Phys. Rev. C* **14**, 2297 (1976).
- [15] S. G. Nilsson, *K. Dan. Vidensk. Selsk. Mat.-Fys. Medd* **29**, No. 16 (1955).
- [16] Rakesh Popli, J. A. Grau, S. I. Popik, L. E. Samuelson, F. A. Rickey, and P. C. Simms, *Phys. Rev. C* **20**, 1350 (1979).
- [17] M. A. J. Mariscotti, G. Scharff-Goldhaber, and B. Buck, *Phys. Rev.* **178**, 1864 (1969).
- [18] C. Michael Lederer, Jack M. Hollander, and Isadore Pearlman, *Table of Isotopes*, 6th Edition (John Wiley and Sons, New York, 1968).
- [19] B. R. Mottelson and S. G. Nilsson, *Mat.-Fys. Skr. Dan. Vid. Selsk.* **1**, No. 8 (1959).
- [20] B. Reehal and R. Sorenson, *Phys. Rev. C* **2**, 819 (1970).
- [21] H.-W. Mueller, *Nucl. Data Sheets* **35**, 281 (1982).